SPECIAL
GDIS Drought Worldwide
COLLECTION

Global Meteorological Drought: A Synthesis of Current Understanding with a Focus on SST Drivers of Precipitation Deficits

SIEGFRIED D. SCHUBERT,[a] RONALD E. STEWART,[b] HAILAN WANG,[a,c] MATHEW BARLOW,[d] ERNESTO H. BERBERY,[e] WENJU CAI,[f] MARTIN P. HOERLING,[g] KRISHNA K. KANIKICHARLA,[h] RANDAL D. KOSTER,[a] BRADFIELD LYON,[i] ANNARITA MARIOTTI,[j] CARLOS R. MECHOSO,[k] OMAR V. MÜLLER,[l] BELEN RODRIGUEZ-FONSECA,[m] RICHARD SEAGER,[n] SONIA I. SENEVIRANTE,[o] LIXIA ZHANG,[p,q] AND TIANJUN ZHOU[p]

[a] *Global Modeling and Assimilation Office, NASA Goddard Space Flight Center, Greenbelt, Maryland*
[b] *Department of Environment and Geography, University of Manitoba, Winnipeg, Manitoba, Canada*
[c] *Science Systems and Applications, Inc., Lanham, Maryland*
[d] *University of Massachusetts Lowell, Lowell, Massachusetts*
[e] *Earth System Science Interdisciplinary Center/Cooperative Institute for Climate and Satellites, University of Maryland, College Park, College Park, Maryland*
[f] *CSIRO Oceans and Atmosphere, Aspendale, Victoria, Australia*
[g] *NOAA/Earth System Research Laboratory, Boulder, Colorado*
[h] *Qatar Meteorology Department, Doha, Qatar*
[i] *International Research Institute for Climate and Society, The Earth Institute, Columbia University, Palisades, New York*
[j] *Climate Program Office, NOAA/Office of Oceanic and Atmospheric Research, Silver Spring, Maryland*
[k] *Department of Atmospheric and Oceanic Sciences, University of California, Los Angeles, Los Angeles, California*
[l] *CEVARCAM, Facultad de Ingeniería y Ciencias Hídricas 5, Universidad Nacional del Litoral and CONICET, Santa Fe, Argentina*
[m] *Departamento de Física de la Tierra, Astronomía y Astrofísica-I, Facultad de Ciencias Físicas, and Instituto de Geociencias (IGEO-CSIC), Madrid, Spain*
[n] *Lamont-Doherty Earth Observatory, Columbia University, Palisades, New York*
[o] *Institute for Atmospheric and Climate Science, ETH Zürich, Zurich, Switzerland*
[p] *State Key Laboratory of Numerical Modeling for Atmospheric Sciences and Geophysical Fluid Dynamics, Institute of Atmospheric Physics, Chinese Academy of Sciences, Beijing, China*
[q] *Collaborative Innovation Center on Forecast and Evaluation of Meteorological Disasters, Nanjing University of Information Science and Technology, Nanjing, China*

(Manuscript received 24 June 2015, in final form 20 January 2016)

ABSTRACT

Drought affects virtually every region of the world, and potential shifts in its character in a changing climate are a major concern. This article presents a synthesis of current understanding of meteorological drought, with a focus on the large-scale controls on precipitation afforded by sea surface temperature (SST) anomalies, land surface feedbacks, and radiative forcings. The synthesis is primarily based on regionally focused articles submitted to the Global Drought Information System (GDIS) collection together with new results from a suite of atmospheric general circulation model experiments intended to integrate those studies into a coherent view of drought worldwide. On interannual time scales, the preeminence of ENSO as a driver of meteorological drought throughout much of the Americas, eastern Asia, Australia, and the Maritime Continent is now well established, whereas in other regions (e.g., Europe, Africa, and India), the response to ENSO is more ephemeral or nonexistent. Northern Eurasia, central Europe, and central and eastern Canada stand out as regions with few SST-forced impacts on precipitation on interannual time scales. Decadal changes in SST appear to be a major factor in the occurrence of long-term drought, as highlighted by apparent impacts on precipitation of the late 1990s "climate shifts" in the Pacific and Atlantic SST. Key remaining research challenges include (i) better quantification of unforced and forced atmospheric variability as well as land–atmosphere feedbacks, (ii) better understanding of the physical basis for the leading modes of climate variability and their predictability, and (iii) quantification of the relative contributions of internal decadal SST variability and forced climate change to long-term drought.

Corresponding author address: Siegfried Schubert, NASA GSFC, 8800 Greenbelt Rd., Greenbelt, MD 20771.
E-mail: siegfried.d.schubert@nasa.gov

DOI: 10.1175/JCLI-D-15-0452.1

1. Introduction

Drought, which can occur in almost any region of the world, is one of the most destructive natural hazards faced by society. Some of the direst concerns related to climate change are associated with possible changes in drought frequency and severity, although regional drought projections often show large uncertainties (e.g., Seneviratne et al. 2012a; Orlowsky and Seneviratne 2013).

A substantial amount of research and operational effort has been devoted to investigating drought. Many drought research studies have focused on particular regions or selected events, whereas others have examined the global distribution of droughts, their forcing factors, and their predictability. Efforts in operational environments now routinely assess current and future drought conditions over a variety of temporal and spatial scales. This broad range of activities, as well as many drought impact studies, suggests a need to document our collective understanding of and capabilities to predict drought. A synthesis of current understanding would help people everywhere benefit as much as possible from existing research and operational capabilities, through, for example, improved decision support and drought mitigation.

The Global Drought Information System (GDIS)[1] addresses these issues. The overall goal of GDIS is to provide coordinated information, monitoring, and prediction of drought worldwide in a user-friendly manner. One of GDIS's objectives is to assess our current understanding of drought and our ability to predict it, thereby identifying research gaps. The present special collection of regionally focused summary articles stems from this component of GDIS. Each article can stand on its own as an important contribution to drought research.

It is also important, of course, to place these summary articles into context and to synthesize some of their findings. This is the goal of the present overview article. To make it tractable, we focus primarily on understanding the role of SST in driving meteorological drought, although some attention is also paid to other drivers as well as temperature anomalies. Furthermore, some of our discussion will focus more generally on seasonal-scale precipitation deficits, given that meteorological droughts can be considered extreme manifestations of such deficits; indeed, the level of deficit required to define a meteorological drought is not set in stone. In discussing such deficits generally, we make the implicit assumption that if a given set of conditions (as identified in this article) leads to a seasonal precipitation deficit, then a more extreme version of these conditions would lead to a more extreme deficit and thus potentially a true meteorological drought. That is, we make the assumption that uncovering the sources of precipitation deficits on seasonal time scales is tantamount to uncovering the sources (if conditions therein were stronger) of meteorological drought.

In this paper we do not address how meteorological drought propagates to agricultural or hydrological droughts, or how soil moisture feedbacks, temperature changes, or human water use act to maintain or even amplify the different types of drought, although these issues are addressed to varying degrees in the articles of the GDIS collection.

Such a focus does not come without limitations; for example, the impact of long-term evapotranspiration changes induced by temperature and radiation changes (e.g., from climate change) may turn out to be as important as (if not more important than) precipitation changes in some regions in producing soil moisture and streamflow deficits at longer time scales (e.g., Cook et al. 2014, 2015). For example, Cook et al. (2014) used CMIP5-driven Palmer drought severity index (PDSI) and standardized precipitation–evapotranspiration index (SPEI; Vicente-Serrano et al. 2010) drought estimates to show that, while robust regional changes in hydroclimate are primarily organized around regional changes in precipitation, increased potential evapotranspiration (PET) computed with the Penman–Monteith approach nearly doubles the percentage of global land area projected to experience significant drying based on these indices by the end of the twenty-first century. Nevertheless, Sheffield et al. (2012), in addressing whether such impacts of increased PET are already evident in recent observationally driven PDSI trends, found that global drought has changed little over the past 60 years [see also Seager and Hoerling (2014) for a discussion of regional differences], indicating that

[1] The GDIS was developed as one of the key recommendations of a WCRP workshop on "Drought Predictability and Prediction in a Changing Climate: Assessing Current Knowledge and Capabilities, User Requirements and Research Priorities," that was held on 2–4 March 2011 in Barcelona, Spain (http://www.clivar.org/sites/default/files/documents/ICPO_162_WCRP_drought_Report.pdf). The capabilities and requirements of the GDIS were further established at a second workshop held in Frascati, Italy, on 11–13 April 2012 (http://www.clivar.org/sites/default/files/documents/GDIS_Report_final.pdf). A third workshop, "An International Global Drought Information System Workshop: Next Steps," was held in Pasadena, California, at the California Institute of Technology (Caltech) campus 10–13 December 2014, and focused on reviewing the GDIS special collection papers and developing the necessary next steps required for moving forward with an experimental real-time global drought monitoring and prediction system (www.wcrp-climate.org/gdis-wkshp-2014-about).

TABLE 1. Temporal correlation between observed annual mean regional mean precipitation (GPCP) and 1) the regional mean annual mean PDSI from Dai et al. (2004) for 1979–2005 and 2) the regional mean annual mean soil moisture (top 100 cm) from the Global Land Data Assimilation System, version 2 (GLDAS-2; Rodell et al. 2004), for 1979–2010. The numbers across the top of the table (1–10) refer to the regions outlined in Figs. 5–8: 1 is the United States and northern Mexico, 2 is northern South America and Central America, and 3 is central South America (Fig. 5); 4 is West Africa, and 5 is East Africa (Fig. 6); 6 is the Middle East, 7 is southern Asia, and 8 is East Asia (Fig. 7); and 9 is Australia, and 10 is Indonesia (Fig. 8).

Region	1	2	3	4	5	6	7	8	9	10
PDSI (1979–2005)	0.52	0.80	0.69	0.66	0.66	0.72	0.69	0.65	0.75	0.71
Soil moisture (1979–2010)	0.72	0.86	0.76	0.70	0.57	0.80	0.66	0.50	0.80	0.81

the focus here on precipitation deficits allows us to address much of the overall drought problem in current climate. Table 1 provides further evidence that such a focus is justified, showing for our selected regions (see section 3) generally high correlations between precipitation and either the PDSI or soil moisture.

We start by providing an overall scientific context for drought through an examination of the global drivers of precipitation and temperature changes on interannual and decadal time scales (section 2). Next, we relate these and other factors to drought in different regions, highlighting implications for predictability and prediction (section 3). Section 4 provides some concluding remarks.

2. Overview of large-scale factors

Here, we review the large-scale or the ultimate (as opposed to the proximate) causes of meteorological drought—the processes responsible for the long-term disruptions of local and regional precipitation-producing phenomena. These processes often act over large distances via various large-scale atmospheric motions such as the Hadley and Walker circulations, Rossby waves, and other atmospheric teleconnection patterns. The forcing for some of these large-scale motions is known to include sea surface temperature (SST) anomalies, land (especially soil moisture) feedbacks, aerosols, and other natural and anthropogenic changes in radiative forcing such as those associated with global warming. These forcings are important because they may provide some degree of drought predictability (e.g., Smith et al. 2012). It must be kept in mind, however, that there is a substantial unforced (i.e., driven by processes internal to the atmosphere) element to the large-scale motions that significantly limits our ability to predict drought at the longer leads.

The various articles in the GDIS drought special collection assess, from a regional perspective, the global processes associated with meteorological drought. We summarize these findings here, while also providing additional background on climate change aspects and regarding meteorological drought on the European continent. In addition, to provide a global framework for our discussion and synthesis, we include a model-based assessment of the dominant large-scale forcing of meteorological drought on seasonal and longer time scales—the response of the atmosphere to SST anomalies (e.g., Hoerling and Kumar 2003; Schubert et al. 2004; Seager et al. 2005). This assessment is based on AMIP-style simulations using prescribed SSTs (see appendix A), with five different state-of-the-art global climate models; results are presented as combined (rather than individual model) statistics. (Individual model results are provided in appendix B.) We provide the model results in each subsection partly to assess their consistency with the findings of the individual special issue GDIS papers. The model results also provide insight into the spatial coherence and seasonality of the forced responses. In examining these results, we must keep in mind that their usefulness may be limited by model deficiencies and by the limitations imposed by employing SST-prescribed integrations.

The link between drought and remote SST anomalies is complicated by the fact that there are different definitions of drought reflecting a wide range of societal (e.g., health, water quality, and political), economic (e.g., agriculture, water supply, transportation, and recreation), and ecosystem (e.g., fish, wildlife, wetlands, biodiversity, and forest fires) impacts.[2] All of these definitions are important. Nevertheless, we focus here on the primary meteorological quantity associated with dry conditions, namely, precipitation. In addition, we also consider conditions in near-surface air temperature, which can affect surface drying through increased evaporative demand in warmer air, although the latter can also result from soil drying associated with meteorological drought itself (e.g., Mueller and Seneviratne 2012; Sheffield et al. 2012; Yin et al. 2014). We begin with an overview of the interannual variability of both precipitation and temperature.

Figure 1 shows the land regions where SST anomalies are expected to influence annual mean precipitation and 2-m air temperature, based on the five atmospheric general circulation models (AGCMs: 12 ensemble members for each) forced with observed SST over the

[2] More information on impacts can be found online (http://drought.unl.edu/Planning/Impacts.aspx).

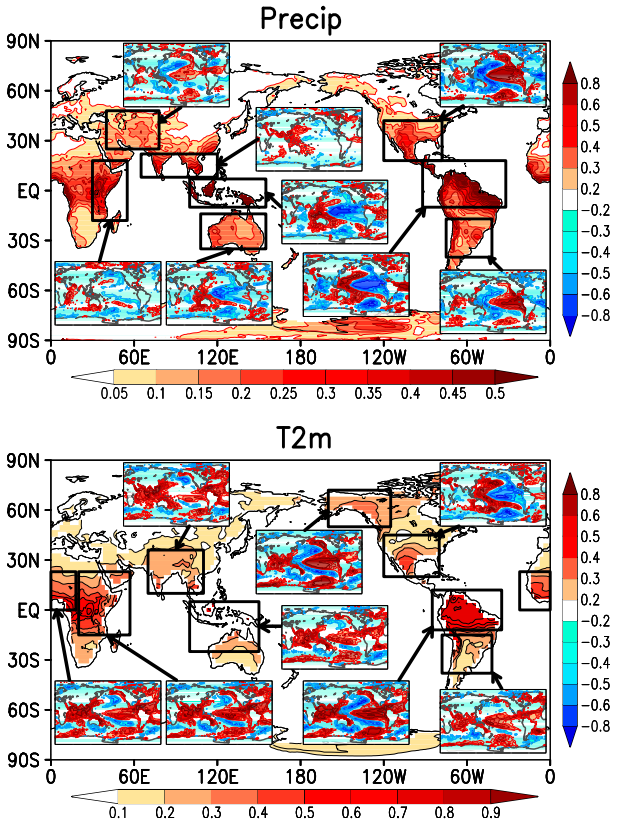

FIG. 1. (top) Background map showing the ratio of two variances: the variance of the ensemble mean time series of annual precipitation and the total variance of annual mean precipitation over all ensemble members (ratios are computed for each model separately and then averaged). Higher values of the ratio indicate a stronger impact of the prescribed SSTs on the precipitation time series. The small inset maps show the correlations between the ensemble mean annual fields (averaged over the boxed areas) with SST (correlations are computed for each model separately and then averaged). All results are for the period 1979–2011 and are based on 60 ensemble members: 12 AMIP simulations for each of five models (GEOS-5, CCM3, CAM4, GFS, and ECHAM5). Results are based on detrended values. (bottom) As in (top), but for 2-m air temperature (note change in contour interval). The horizontal color bars are for the variance ratios, and the vertical color bars are for the correlations.

period 1979–2011. (See appendix A for descriptions of the models and their simulations.) The base maps show the fraction of the total interannual variance that is forced by SST. Focusing on precipitation (Fig. 1, top), we see that the ratios outside the tropics (poleward of 30°N and 30°S latitude) are generally quite small (<0.2)[3]; outside the tropics, much of the interannual variability is unforced by SST and is therefore likely to be unpredictable from SST forcing at interannual time scales. This is for instance the case in northern Eurasia, central Europe, and central and eastern Canada. We note nonetheless that (agricultural and hydrological) drought predictability in these regions may be arising from year-to-year memory in soil moisture and/or snowpack, or possibly interannual changes in radiative forcing, aspects that we do not consider in the present review. The largest fractions of interannual precipitation variability explained by SST in the midlatitudes occur over the U.S. southern Great Plains, southwest Asia, parts of Australia, and South America. Values exceed 0.3 primarily in tropical land areas, including northwest South America, Indonesia, Central America, Southeast Asia, southwestern India, and eastern Africa. The fractions for 2-m temperature (T2m; Fig. 1, bottom) are generally considerably larger than those for precipitation. Some regions in the extratropics show values exceeding 0.4 (e.g., southern U.S. Great Plains and Mexico). Nevertheless, the largest values are again confined to the tropical regions of Africa, southern Asia, Indonesia, and much of the northern half of South America, with values sometimes exceeding 0.7.

El Niño–Southern Oscillation (ENSO) is a key player in the development of precipitation deficits in many regions of the world (e.g., Ropelewski and Halpert 1987). Figure 1, in addition to showing the fraction of interannual variance forced by SST, shows how SST is correlated with precipitation (Fig. 1, top) and T2m (Fig. 1, bottom) within selected regions (small inset maps in Fig. 1)[4]; the patterns show a clear link to ENSO and to SST in general. We will refer to these maps as we review the results from the individual contributions to this special collection.

A number of regions of the world have suffered multiyear drought (e.g., beyond the ENSO time scale), and one may wonder whether such droughts result from naturally occurring decadal modes of variability [e.g., the Atlantic multidecadal oscillation (AMO) and Pacific decadal oscillation (PDO)], from decadal changes in the relationships between interannual modes of variability

[3] We note that values of the ratio greater than 0.06 are statistically significant at the 1% level based on an F test following Zwiers et al. (2000).

[4] We emphasize that these are meant to be summary results. As we shall see in section 3, there are in some cases considerable variations in SST connections within a box and between seasons. For example, the western portions of East Africa tend to have a June–September (JJAS) rainfall maximum, and El Niño is tied to drought. Farther east (eastern Ethiopia, Kenya, and Somalia) the rainy season is bimodal with drought associated with La Niña (and its influence on Indian Ocean SSTs) during boreal fall. The ENSO signal reverses sign between eastern and southern Africa as well, with 15°S frequently considered the northern limit of the southern African region.

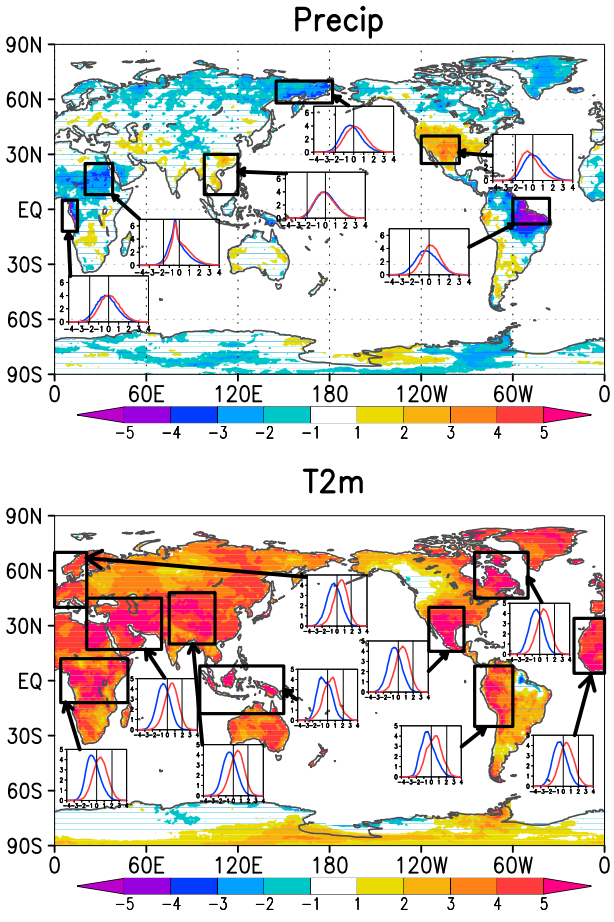

FIG. 2. The shift in probabilities of extremes between the two periods 1998–2011 and 1979–93 defined as $[P(x_2 > x_c) - P(x_1 > x_c)]/P(x > x_c)$, where x_2 refers to values during the recent period (1998–2011) and x_1 refers to values during the earlier period (1979–93). The shift is normalized by $P(x > x_c)$, where x refers to values during the entire time period, and x_c is chosen so that $P(x > x_c)$ is 2.5%. Results are for (top) precipitation and (bottom) 2-m temperature; in the case of precipitation, the shift in probability actually refers to the left tail of the distribution (values less than x_c). The results are based on 12 ensemble members for each of five models (GEOS-5, CCM3, CAM4, GFS, and ECHAM5). Each model's values are first normalized to have zero mean and unit variance. The inset plots show the actual pdfs for the two periods (red is for the recent period and blue indicates the earlier period) for all grid points in the indicated boxes (land only). Vertical lines highlight the zero value and the value of x_c.

[e.g., ENSO and Atlantic El Niños (Losada et al. 2012)], from global warming (Mohino et al. 2011a), or from no mechanism at all (i.e., from a simple random sequence of dry years generated from internal atmosphere variability). In Fig. 2 we provide a global depiction of the changes that have occurred over the last three decades in the tails of the probability distributions of 2-m temperature and precipitation based on the same set of AGCM runs used to produce the results in Fig. 1. Here, we show how the probability of exceeding (or falling short of, in the case of precipitation) a particular critical value x_c has changed between the first and last 15 years of the record. Because we are focusing on extreme years, x_c is chosen to be the 2.5% value based on all 33 years [i.e., the value that would be exceeded (or fallen short of) on average only 2.5% of the time]. The last three decades, we note, are characterized by both global warming and shifts in the AMO and PDO (Fig. 3), so anthropogenic forcing and natural variations may both contribute significantly to observed regional changes between these two periods.

In regard to precipitation (Fig. 2, top), the models indicate that much of the United States has experienced an increase in the probability of extreme dry years during the last three decades (particularly the central plains). Here, the shift is 1–1.5 times the climatological probability of 2.5%. The shift is clear in the probability density functions (pdfs) provided in the inset plots of Fig. 2. As we shall see next, this shift reflects forcing by SST with a strong decadal component and does not necessarily indicate a long-term trend. In fact, if a longer time period is considered, the United States (especially the central part of the country) has generally experienced wetter conditions compared to the 1950s (e.g., Wang et al. 2009; Seneviratne et al. 2012a; Hartmann et al. 2013; Greve et al. 2014). As Wang et al. (2009) showed, even for this longer time, period the precipitation "trend" is still dominated by SST forcing with decadal time scales.

Parts of Indochina and southeastern China also experienced an increase in the probability of extreme dry years. In contrast, northeastern South America shows a substantial decrease in the probability of dry years over the last three decades, although with little change in the probability of extreme wet years (see inset plots of Fig. 2). The tropical west coast of Africa, the Sahel, and northeastern Russia also show a reduction in the probability of extreme dry years. The pdf characterizing precipitation in northeastern Africa shows no shift in the peak, so that the changes in the pdf occur primarily in the tails. In general, for the Northern Hemisphere during the last three decades, the high latitudes show a tendency for a reduction in the probability of dry years, whereas the midlatitudes (including parts of Europe, southern Asia, and the United States) show a tendency for an increase in the probability of dry years. In the Southern Hemisphere, the probability of extreme dry years is increased in parts of southern Africa, Australia, and southern and western South America and is mostly decreased in tropical regions.

Relative to precipitation, the results for 2-m temperature (Fig. 2, bottom) are more homogenous, with almost all regions of the world showing an increase in the probability of very warm years over the last three

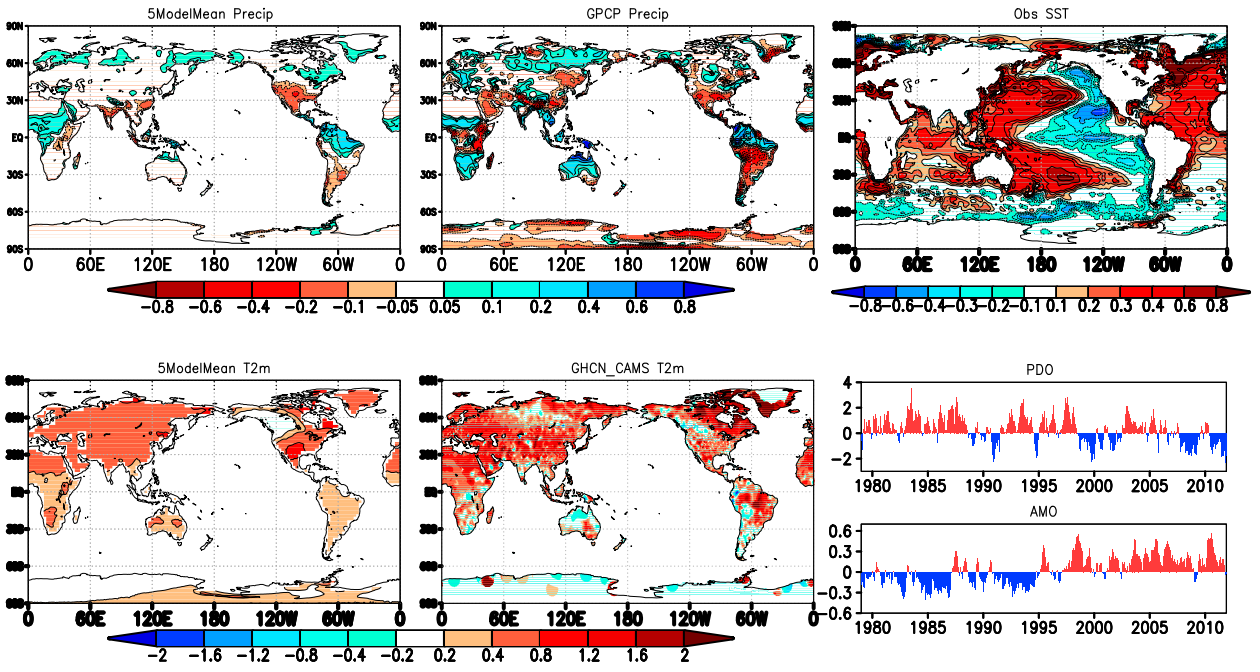

FIG. 3. (top left) Mean simulated precipitation differences (mm day^{-1}) between 1998–2011 and 1979–93, based on results from the five models. (bottom left) Corresponding differences in T2m (°C; land only). (center) As at (left), but for the observations. (top right) The mean observed SST differences (°C) between 1998–2011 and 1979–93. (bottom right) The time series of the PDO (http://research.jisao.washington.edu/pdo/PDO.latest) and AMO (http://www.esrl.noaa.gov/psd/data/timeseries/AMO/).

decades (see also Hartmann et al. 2013). Regions where the increase in probability exceeds twice the climatological probability of 2.5% include the south-central United States, Mexico, northwestern South America, eastern Canada, parts of Europe, southern Asia, Japan, tropical and northern Africa, Indonesia, and southern Australia. Only northeastern South America and western Canada show substantial regions with little increase (and even some scattered regions of decrease) in the probability of warm years. The inset plots of Fig. 2 show that these changes largely result from a shift in the mean rather than from a change in the shape of the pdfs for the analyzed regions.

Figure 3 compares the simulated and observed mean changes between the two periods. The model results show warming everywhere except over northwestern North America and northeastern South America, with the strongest warming occurring in the Northern Hemisphere. The model results are generally consistent with the observed temperature changes, although they are smoother as a result of being an average over 60 ensemble members. There are also strong similarities between the simulations and observations in the precipitation differences, with both difference maps showing decreases over the United States and increases over northern South America, northern Australia, northern Eurasia, and central Africa. Some differences in the estimated precipitation changes, however, do appear, including over central South America (observed decreases not found in the simulations), India, and Southeast Asia. The extent to which these reflect model deficiencies or sampling differences associated with unforced internal atmospheric noise is unclear. Overall, the changes are consistent with the changes in the pdfs discussed earlier. They appear to reflect, in part, a response to SST changes linked to the PDO, the AMO, and a warming trend (Fig. 3; see also Schubert et al. 2009), as well as possible direct impacts on the atmosphere from increasing greenhouse gases (GHGs).[5]

3. Causes of meteorological drought by region

We now provide a more in-depth discussion of meteorological drought for specific regions. While much of the discussion is condensed from the individual contributions to this special collection, we also present relevant results from the aforementioned SST-forced AGCM simulations, as well as results from other key studies where necessary to address issues not covered by the individual contributions.

[5] All of the AGCMs (except for CCM3) were forced with observed GHGs (appendix A).

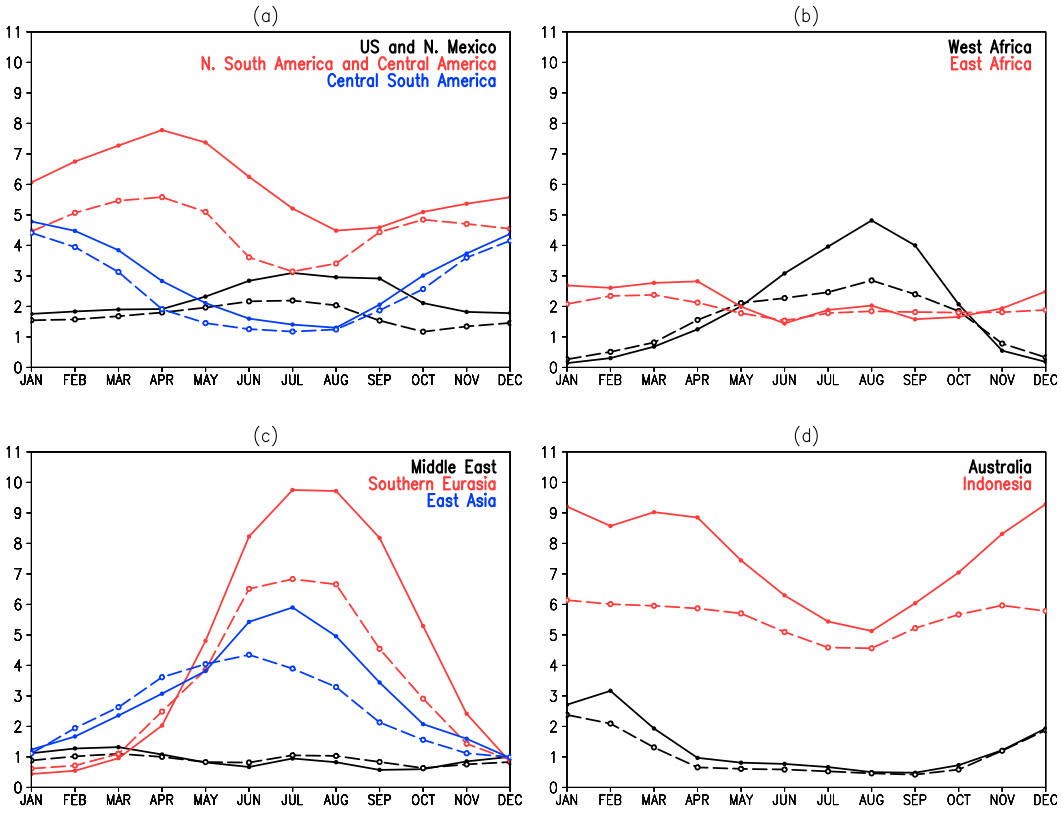

FIG. 4. Observed (GPCP; solid lines) and simulated (five-model ensemble mean; dashed lines) annual cycle of precipitation (mm day^{-1}) for the selected regions based on the period 1979–2011. [The regions are those examined in Figs. 5–8 (see the boxes outlining the regions in those figures)].

We begin by providing in Fig. 4 a brief assessment of the ability of the models to produce the observed annual cycle of precipitation in each of the selected regions (see the boxes in Figs. 5–8 for the definitions of the regions). This is also meant to facilitate the following discussion about the links to SST, by giving the reader an assessment of the timing of the wet and dry seasons in each region. Overall, the models do a reasonable job in reproducing the observed annual cycle, although the peak rainfall tends to be underestimated especially in the tropical land regions (northern South America–Central America, southern Eurasia, and Indonesia).[6] It is noteworthy that the Central and South American region (Fig. 4a) shows some evidence of the well-known midsummer drought found over Mexico and Central America (e.g., Magaña et al. 1999), something that is also reproduced in the model results. We also note that the spatial averaging tends to hide any regional differences. This is especially true for the East African region, which shows a rather flat annual cycle (Fig. 4b), despite having local rainfall regimes that include unimodal (JJA and DJF maxima) and bimodal [MAM and October–December (OND) maxima] annual cycles (see section 3c).

a. North America

The occurrence of precipitation deficits over North America on annual time scales is predominantly associated with SST variability in the tropical Pacific (e.g., Seager et al. 2005), with some contribution from SST variability in the Atlantic (e.g., Schubert et al. 2009). Figure 1 (top) shows that precipitation deficits are largely tied to La Niña conditions, with the largest impacts in the southern Great Plains and northern Mexico. La Niña conditions also lead to warming across the southern plains and much of the U.S. Southeast, whereas El Niño conditions are associated with warming over Alaska and northwestern Canada (Fig. 1, bottom).

These results are consistent with the in-depth assessment of the causes of North American drought carried out by Seager and Hoerling (2014). Using a subset of the

[6] We note that including the ocean points when computing the area averages of the precipitation in these regions produces much closer agreement between the observations and model results (not shown), indicating the underestimation of the precipitation is confined to the land areas.

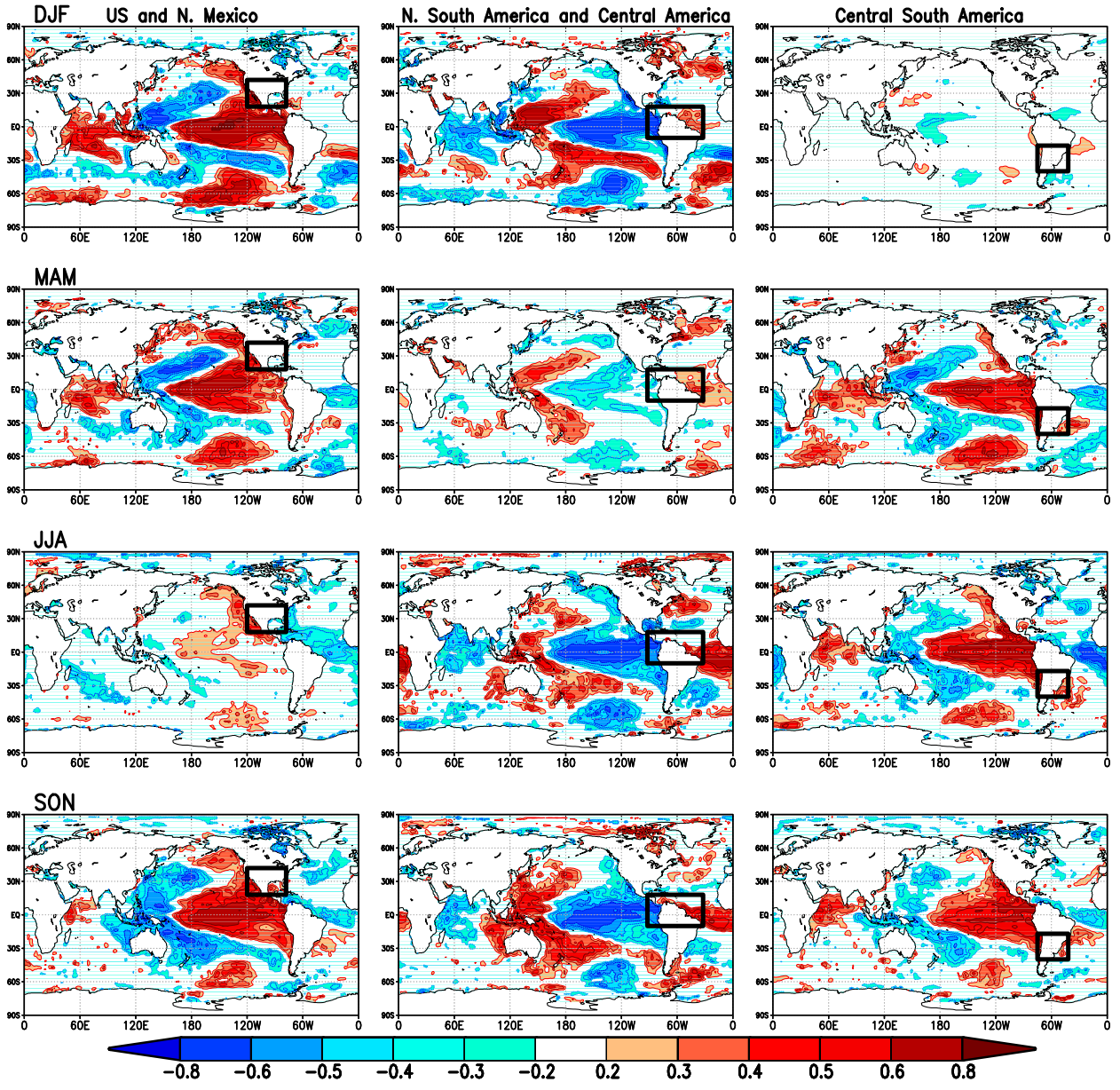

FIG. 5. (left) The correlations between the ensemble mean precipitation averaged over the United States and northern Mexico (black box) and SST for individual seasons (correlations are averaged over the five models). (center) As at (left), but for northern South America and Central America (black box). (right) As at (left), but for central South America (black box).

climate models underlying Fig. 1, Seager and Hoerling (2014) find that SST forcing of annual mean precipitation variability accounts for up to 40% of the total variance in northeastern Mexico,[7] the southern Great Plains, and the Gulf Coast states but less than 10% in central and eastern Canada. They further find that, in addition to the tropical Pacific, tropical North Atlantic SST contributes to the forcing of annual mean precipitation and soil moisture in southwestern North America and the southern Great Plains.

Seager and Hoerling (2014) find that SST forcing was indeed responsible for multiyear droughts in the 1950s and at the turn of the twenty-first century. Attribution to SST patterns, however, is not always straightforward. Wang et al. (2014) highlight how the responses over North America to SSTs in different ocean basins can reinforce each other or cancel out, complicating the

[7] Mexico will be discussed further in the following section.

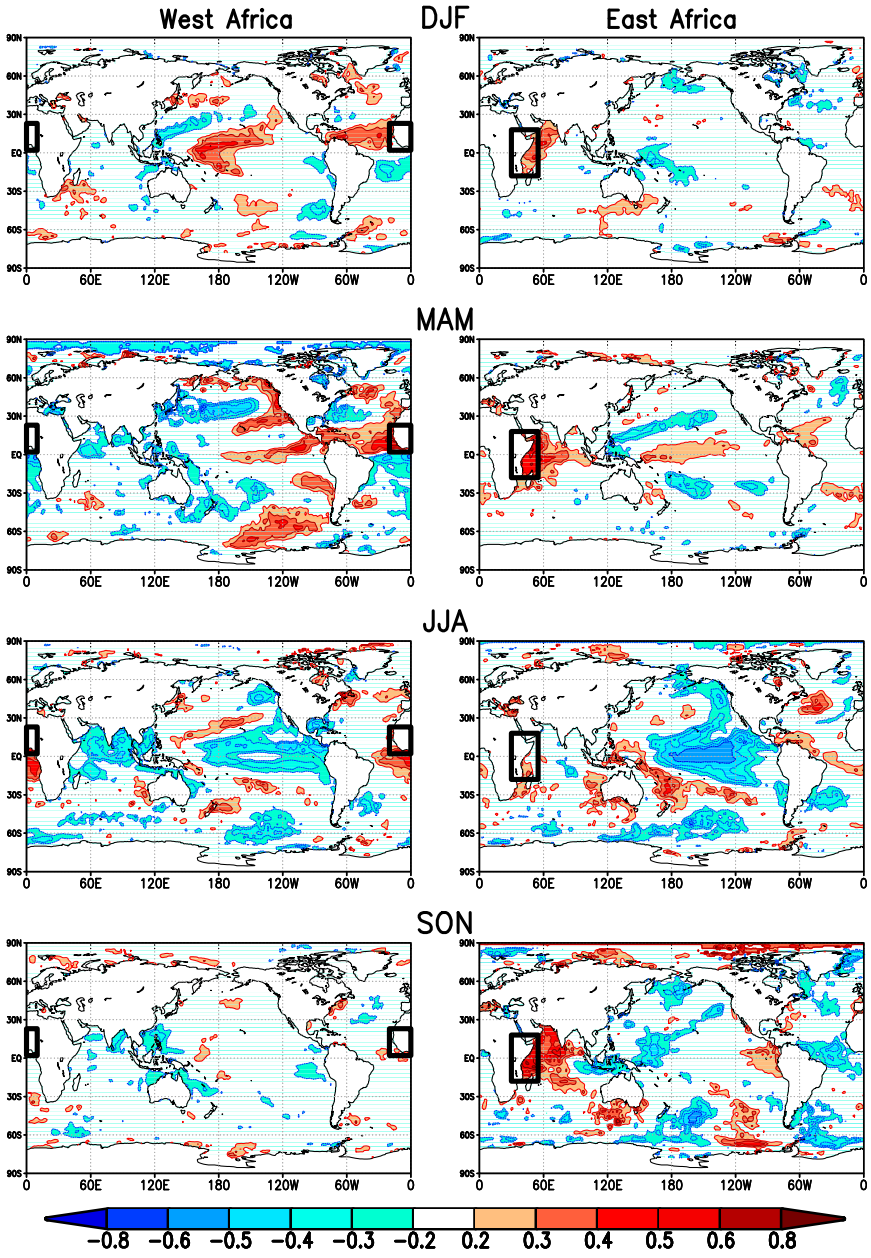

FIG. 6. (left) The correlations between the ensemble mean precipitation averaged over West Africa (black box) and SST for individual seasons (five-model mean). (right) As at (left), but for East Africa.

analysis of SST impacts. Atmospheric internal variability also muddies the signal; internal atmospheric variability can contribute significantly to extreme droughts, especially on shorter (monthly) time scales (Seager et al. 2014a; Hoerling et al. 2014; Wang et al. 2014). For example, the most extreme phase of the Texas drought in 2011 was largely unforced by SST, and the central plains drought of 2012 showed almost no contribution from SST forcing.

Figure 5 (left) shows, for the United States and northern Mexico, the seasonality of the link between precipitation and SST, as determined from the model simulations. The most striking aspect of this seasonality is the strong ENSO connection for all seasons except JJA, although the strong connection in MAM is not supported by the observations (see Fig. B5). Summertime precipitation is negatively correlated with tropical Atlantic SST, a result consistent with Kushnir et al. (2010) and Wang et al. (2008), who

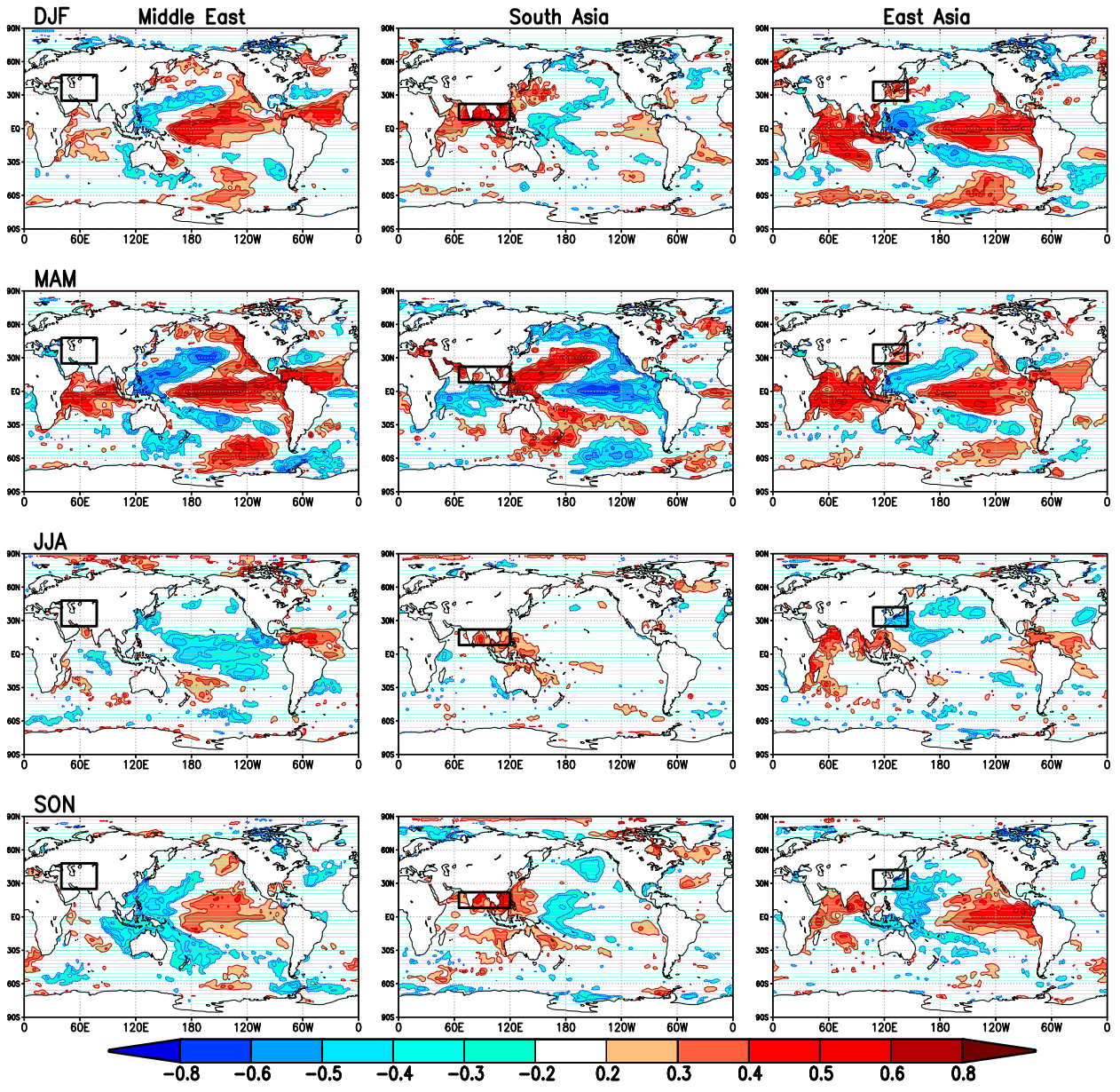

FIG. 7. (left) The correlations between the ensemble mean precipitation averaged over the Middle East (black box) and SST for individual seasons (five-model mean). (middle) As at (left), but for southern Asia. (right) As at (left), but for East Asia.

showed that a larger Atlantic warm pool leads to a suppressed Great Plains low-level jet and associated reduced central U.S. precipitation. On the other hand, summertime precipitation is positively (although weakly) correlated with SST along the west coast of North America extending into the central tropical Pacific, with a structure reminiscent of the PDO. The link to the Indian Ocean also has substantial seasonality, with positive correlations during DJF and MAM and negative correlations extending westward from the warm pool into the eastern Indian Ocean during SON.

Seager and Hoerling (2014) show that, during the early twenty-first century, natural decadal variations in tropical Pacific and North Atlantic SSTs have contributed to a dry regime for the United States (see also Fig. 3). Since the mid-1990s, both the PDO and the AMO have gone through striking decadal transitions (Fig. 3) to a cold tropical Pacific–warm North Atlantic that is "ideal" for North American drought (Schubert et al. 2009). Figure 2 indicates that in the southern plains region, the drier regime is associated with a substantial increase in the probability of extreme dry years. In addition, Seager and Hoerling (2014)

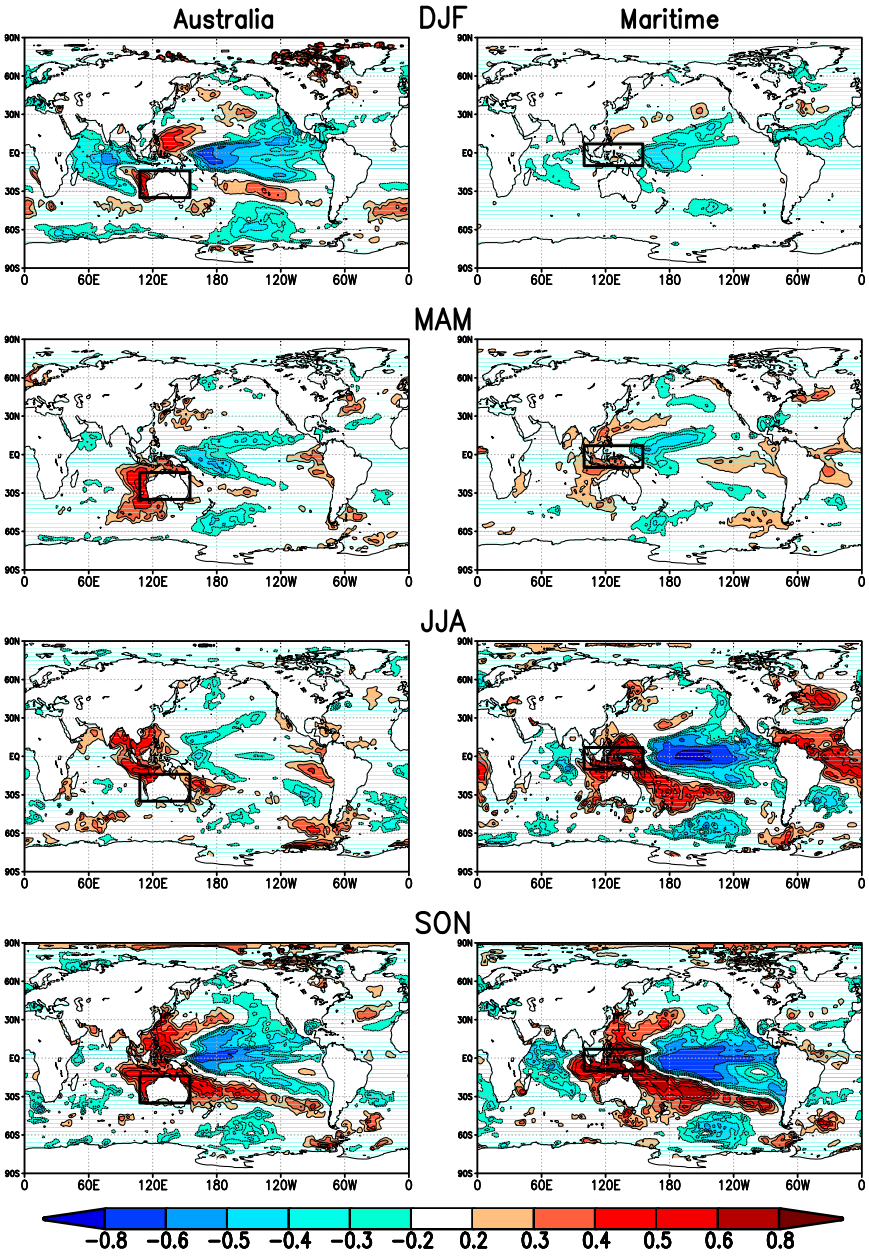

FIG. 8. (left) Correlations between the ensemble mean precipitation averaged over Australia (black box) and SST for individual seasons (five-model mean). (right) As at (left), but for the Maritime Continent.

note that long-term changes caused by increasing trace gas concentrations are now contributing to a modest signal of soil moisture depletion, mainly over the U.S. Southwest, thereby prolonging the duration and severity of naturally occurring droughts.[8]

Understanding the extent to which precipitation and air temperature variability is determined by SST forcing (potentially providing predictability) and internal atmospheric variability (providing no predictability on seasonal and longer time scales) is an important research challenge (e.g., Wang et al. 2014). Recently the 2011–14 California drought has been linked to a localized warm SST anomaly in the western tropical Pacific (Seager et al. 2014c; Hartmann 2015), which raises the important

[8] Water pumping is another source of drying in the southwestern United States.

issue of the forcing of drought over North America by Pacific SST anomaly patterns other than ENSO. The contribution of soil moisture to the variability is also still poorly understood, as reflected by the substantial differences in the strength of land–atmosphere feedback and the soil moisture memory simulated by current climate models (e.g., Koster et al. 2004; Seneviratne et al. 2006). Also poorly understood is the nature and predictability of the unforced component [e.g., internal atmospheric variability associated with Rossby waves and other atmospheric teleconnections, especially during the summer (Schubert et al. 2011)].

Regarding changes under enhanced greenhouse gas concentrations and global warming, the additional forcing of increasing radiation could lead to enhanced evapotranspiration during drought events. Climate projections for the end of the twenty-first century suggest a robust increase in soil moisture drying in the southern United States and Mexico, whereas signals for accumulated precipitation deficits are less robust across climate models (Orlowsky and Seneviratne 2013). However, historical records do not yet suggest a detectable signal in North America, either in precipitation or precipitation–evapotranspiration (Hartmann et al. 2013; Greve et al. 2014). How the SST impacts may change in a warming world is largely unknown.

b. *Latin America*

Figure 1 shows that SST impacts on temperature and precipitation are strong over northern South America; these signals are largely associated with ENSO and tropical Atlantic variability (e.g., Mechoso and Lyons 1988; Saravanan and Chang 2000; Giannini et al. 2004). Via this connection, this region may see substantial improvements in seasonal prediction skill as climate models improve (e.g., Folland et al. 2001; Goddard et al. 2003). In Central America, as in northern South America, precipitation is correlated negatively with tropical Pacific SST and positively with tropical Atlantic SST. Indeed, the extent to which the Atlantic signals are independent of ENSO is still not fully quantified (e.g., Chang et al. 2003). Extreme droughts in northeastern Brazil have been linked to very strong El Niño events (McCarthy et al. 2001). Conversely, western Amazon droughts depend on tropical North Atlantic SST anomalies more than on ENSO (Marengo et al. 2008). Further analysis demonstrated that the tropical North Atlantic influence is largest during dry season droughts in the southern Amazon, but ENSO still has a stronger influence during the wet season for the entire basin (Yoon and Zeng 2010).

Figure 1 also shows that relatively strong signals for precipitation over South America extend south along the west coast, which shows enhanced precipitation associated with La Niña conditions. Relatively high temperature signals along the west coast extending southward into northern Chile are associated with positive correlations with El Niño. The east coast over southern Brazil and Uruguay, including northern and central Argentina (much of the La Plata River basin), has reduced precipitation associated with La Niña conditions (Diaz et al. 1998; Fig. 1, top). According to McCarthy et al. (2001), during La Niña events Chile and central-western Argentina exhibit negative anomalies of rainfall and snowfall leading to reduced summer streamflow.

Figure 5 illustrates the seasonality of the link to SST over northern South America and Central America (Fig. 5, center) and over central-southern South America (Fig. 5, right). For the former region, the aforementioned link to the El Niño cycle is weakest during March–May (MAM), and the link to the tropical Atlantic is strongest during June–August (JJA) and September–November (SON). On the other hand, Cazes-Boezio et al. (2003) show that the ENSO impact on precipitation in Uruguay occurs primarily during austral spring (October–December), but is almost absent during peak summer (January–February), followed by weak impacts during March–July. This is consistent with our much larger central-southern South American region (and with somewhat different definitions of the seasons), which is characterized by reduced (enhanced) precipitation in association with La Niña (El Niño) conditions for all seasons except December–February (DJF), when correlations with SST are negligible.

Although droughts in southeastern South America exhibit a strong dependence on La Niña (cold Pacific), a warm tropical North Atlantic can help define the shape and intensity of the drought episodes (Seager et al. 2010; Mo and Berbery 2011). Notably, the effect of land surface–atmosphere interactions, in the form of soil moisture–precipitation coupling, is essential in the development of drought in southern South America (Xue et al. 2006; Wang et al. 2007; Ma et al. 2010; Sörensson and Menéndez 2011). Barreiro and Diaz (2011) noted that improved seasonal forecasts over South America require the proper representation of the teleconnection processes and regional land–atmosphere interactions need to be adequately resolved. Müller et al. (2014) showed that during the severe 2008 drought in southern South America, a realistic representation of land surface biophysical properties leads to a better depiction of surface–atmosphere processes that consequently reduces model biases and eventually contributes to improved prediction skill of droughts.

McCarthy et al. (2001) note that in Central America topography influences the ENSO impacts. During El

Niño years, the Pacific side is characterized by reduced precipitation, while some parts of the Caribbean side have above normal rain. They also note that over Colombia El Niño events are associated with reductions in precipitation, streamflow, and soil moisture, whereas La Niña is associated with heavier precipitation and floods (Poveda and Mesa 1997), especially during December–January. El Niño also tends to bring large positive precipitation anomalies to the eastern part of the Andes, Ecuador, and northern Peru.

Future climate scenarios produced by regional downscaling suggest a precipitation decrease over the tropical region of South America, with an increase over the subtropical areas (Sánchez et al. 2015). In relation to extremes, climate change scenarios for South America suggest an increase in dry spells, with more frequent warm nights (Marengo et al. 2009).

c. *East Africa*

Lyon (2014) provides a review of the regional and large-scale SST and atmospheric circulation patterns associated with meteorological drought in East Africa on seasonal and longer time scales. Analysis of drought in the region is complicated by local rainfall regimes that generally consist of unimodal (JJA and DJF maxima) and bimodal (MAM and OND maxima) annual cycles. On seasonal-to-interannual time scales, ENSO is the largest source of seasonal rainfall variations, but depending on season and location, it has opposite effects: La Niña is frequently associated with drought during the OND ''short rains'' in the central and eastern areas of the greater Horn of Africa (this is not well captured by most of the models; see Figs. 6 and B1), whereas El Niño is linked to deficient rainfall during boreal summer in locations farther west having a unimodal annual cycle (consistent with Fig. 6). Particularly for the short rains, the Indian Ocean plays a critical role in mediating the impact of ENSO, with the development of a west–east Indian Ocean SST anomaly dipole pattern (IOD) being closely associated with rainfall variations (see also Fig. 6). ENSO, however, is associated with at most roughly 25% of the interannual variations in East African rainfall (consistent with Fig. 1).

In observations, interannual variations in MAM ''long rains'' (Funk et al. 2008; Lyon and DeWitt 2012) in East Africa do not show a statistically significant correlation with SSTs in any ocean basin (generally consistent with Fig. 6, although the models do show positive correlations with SST in the western Indian Ocean). At longer time scales, AMIP-style model runs do tend to capture the decline in the East African long rains associated with the shift in Pacific SSTs toward the cool phase of the PDO in 1998/99 (Lyon 2014; Yang et al. 2014; see also Figs. 3 and 9). The models may thus respond more to decadal, rather than interannual, variations in SSTs. Liebmann et al. (2014) suggest this result may be tied to the relative magnitudes of multidecadal SST fluctuations relative to interannual variability.

On longer time scales, there is growing concern over an observed increase in the frequency of drought, primarily during the MAM long rains. This increase has had dire impacts across the greater Horn of Africa, with the most recent drought in 2010/11 helping to trigger a humanitarian crisis and contributing to the fatalities of tens of thousands of people. The increase in drought frequency has raised concerns about the possible role of anthropogenic climate change. Paradoxically, the consensus of climate model projections is for the region to become wetter during the current century in response to anthropogenic greenhouse gas forcing (IPCC 2007). Lyon et al. (2014), Lyon (2014), and Yang et al. (2014) provide evidence that the recent rainfall decline is substantially driven by natural, multidecadal variability, a result consistent with our model simulations (Fig. 9). Consistent with Lyon and DeWitt (2012), subsequent studies by Hoell and Funk (2013, 2014) suggest that long-term anthropogenic warming of the western Pacific may further enhance the equatorial SST gradient associated with the cold phase of the PDO and thus also enhance drying in East Africa during MAM. As to whether East Africa will become wetter or drier as a result of anthropogenic forcing, Yang et al. (2014) caution that most coupled climate models do not properly capture either the observed annual cycle of rainfall in East Africa or the observed relationship between seasonal rainfall variations and SSTs in different basins (particularly the Indian Ocean), calling into question the reliability of climate projections in East Africa. Lyon (2014) concludes that the hydroclimatic response of East Africa to anthropogenic climate change remains an open question and that more research is needed to better understand the physical processes associated with the rainfall variability of the region across multiple time scales.

d. *West Africa and Sahel*

Rodríguez-Fonseca et al. (2015) focus on rainfall variability across multiple time scales in West Africa and the Sahel. They conclude that SST variations are largely responsible for rainfall variability in the region. Land surface processes and aerosols including those from volcanic eruptions modulate the SST influence.

Figure 6 (left) indicates a strong seasonality in the correlation between West African (including western Sahel) rainfall and SST in the simulation by the five models with the prescribed SST corresponding to the observed over the period 1979–2011. During the rainy

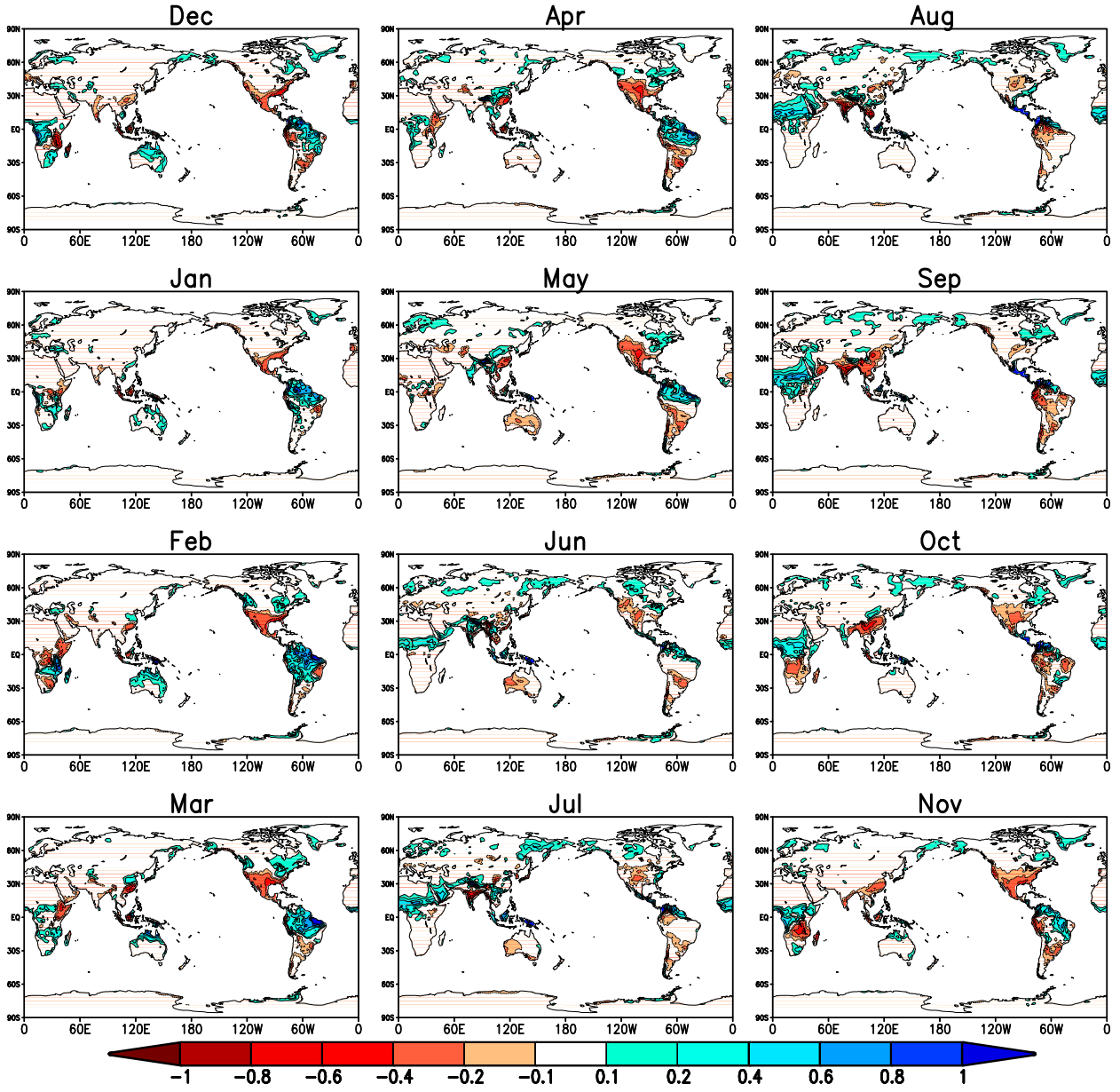

FIG. 9. The five-model mean simulated precipitation differences between 1998–2011 and 1979–93 for individual months (mm day^{-1}).

season (JJA), increased precipitation over West Africa is associated with colder SST in the eastern tropical Pacific and northern Indian Ocean, and with warmer SST in the tropical Atlantic–Gulf of Guinea. During the dry season (DJF), when climatological precipitation is small, increased precipitation is associated with warmer SST in the tropical Atlantic–Gulf of Guinea, as well as in the tropical North Atlantic and central tropical Pacific. Correlations are weaker and less organized in the Pacific during MAM, and little connection with SST is apparent during SON.

Other experiments using AGCMs with prescribed SSTs in individual ocean basins have provided additional insight. During the wet season, warm equatorial SST anomalies corresponding to a warm Atlantic El Niño (Rodríguez-Fonseca et al. 2009) are associated with precipitation increases over the Gulf of Guinea and weaker decreases over the Sahel. The impact of a Pacific warm event varies during the season. In the early part of the season (May–June) warming of the equatorial Pacific reduces rainfall over the Gulf of Guinea and enhances it over the Sahel. In the late part of the wet

season (July–August) warming of the equatorial Pacific reduces rainfall over the Sahel. In the seasonal mean, the negative effects of the Pacific El Niños in the late season prevail over the positive ones in the early period, as shown in Fig. 6.

Rodríguez-Fonseca et al. (2015) discuss a unique aspect of the West African rainfall variability at interannual time scales: its links with the variability of tropical SSTs have shown nonstationary features (see also Rodríguez-Fonseca et al. 2011 and Mohimo et al. 2011b). Pacific cold events and Atlantic warm events tend to appear simultaneously after the 1970s (Rodríguez-Fonseca et al. 2009). AGCM experiments demonstrate that, during this period, the impacts of simultaneous SST anomalies in the Indo-Pacific and Atlantic on Sahel rainfall tend to cancel each other such that the north–south dipole in rainfall anomalies over West Africa expected from Atlantic SST anomalies alone does not appear in the observations (Losada et al. 2012).

Analysis of observational data and model results has provided clues on the mechanisms at work in the connections described above. Anomalous warming of the southern tropical Atlantic enhances ascent over the Gulf of Guinea and descent over the Sahel. A warming in the Pacific and Indian Oceans generates equatorial Rossby waves that contribute to subsidence over the Sahel and thus to reduce regional precipitation. In addition, Mediterranean warm events are linked to increased moisture flux convergence over the Sahel.

Decadal SST variability and global warming are also relevant to Sahelian drought. In recent decades the Sahel has been recovering from a devastating drought in the 1970s and 1980s. It has been suggested that a special combination of three different modes of SST variability (the global warming trend, the positive phase of the interdecadal Pacific oscillation, and the negative phase of the AMO) led to this drought (Mohino et al. 2011a). Vegetation dynamics has been contributing to regional climate persistence (e.g., Zeng et al. 1999). The recovery from the drought appears to be driven by SST also, as a similar feature is obtained in SST-forced model simulations. Regarding global warming, Rodríguez-Fonseca et al. (2015) note that, while rainfall projections have a large spread, models do show a tendency for slightly wetter conditions over the central Sahel and drier conditions over the west. The onset of the rainy season is projected to be delayed, especially over West Africa, while more abundant precipitation is expected during the late rainy season.

Rodríguez-Fonseca et al. (2015) caution that more research is needed to further support these model-based findings on the variability of Sahel rainfall. Although most models capture, for example, the link with Mediterranean SSTs, some important teleconnections are still not well reproduced [e.g., those linked to equatorial Atlantic SSTs and Pacific ENSO (Rowell 2013)]. Also, coupled atmosphere–ocean general circulation models have difficulties in correctly reproducing the seasonal cycle and variability of the tropical Atlantic SST [including the Atlantic equatorial mode (Richter 2015)] and the Pacific (e.g., Mechoso et al. 1995).

e. *The Middle East and southwest Asia*

Barlow et al. (2016) provide a comprehensive review of our current understanding of drought in the Middle East and southwest Asia—a region that is water-stressed, societally vulnerable, and prone to severe droughts. They note that this understanding is still at an early stage, although it appears that large-scale climate variability, particular La Niña in association with a warm western Pacific, contributes to region-wide drought, including the two most severe droughts of the last 50 years (1999/2001 and 2007/08). Barlow et al. (2016) provide a schematic for those two years indicating how La Niña–related SSTs and a warm western Pacific led to wave responses that affected vertical motion, moisture flux, and storm tracks in the region. They note that the North Atlantic Oscillation (NAO), the AMO, and the Atlantic SST tripole pattern also influence the region, although the strength of the teleconnections varies considerably within the region, and the temporal stability of the relationships is somewhat uncertain.

Figure 1 (top) highlights the role of ENSO (and perhaps the PDO) in influencing drought in southwest Asia on annual time scales. This result shows some model dependence but appears to be consistent with observations (Fig. B2). Figure 7 (left) shows that there is a strong seasonality to the precipitation–SST connection in this region, with the strongest correlations in MAM (La Niña, together with a cool tropical Indian Ocean and cool tropical North Atlantic, is apparently conducive to drought conditions then) and similar, although somewhat weaker (especially in the tropical Indian Ocean) correlations in DJF. These two seasons comprise the wet season for most of the region, associated with synoptic precipitation (Barlow et al. 2016). Warm season precipitation is important in Pakistan and along the southern coast of the Arabian Peninsula, associated with the Indian monsoon and the ITCZ. During JJA the link to SST changes sign in the tropical Pacific, so that reduced precipitation is linked to warm tropical Pacific SSTs together with cold SSTs in the tropical Atlantic. SON shows the beginnings of the cold-season link to ENSO, with a coherent ENSO pattern extending from the western Mediterranean region to southwest Asia (Mariotti 2007).

Barlow et al. (2016) note that in the high mountains of the region, snowmelt provides predictability for peak river flows and potentially for vegetation; vegetation in the region is closely linked to precipitation and may also play a feedback role. The drying of the eastern Mediterranean region is a robust feature of future projections, as are temperature increases.

f. East Asia

Zhang and Zhou (2015) review drought over East Asia with a primary focus on China. They point out that because of the seasonal variation of the monsoonal circulation, drought mostly occurs over northern and southwestern China in spring, with the highest drought frequency and maximum duration occurring during that season. In early July, drought tends to occur in the Yangtze and Huaihe River valleys of China and also across Korea and Japan as a result of the influence of the northwestern Pacific subtropical high.

The interannual variability of East Asian summer monsoon (EASM) precipitation is in part associated with the Pacific–Japan teleconnection pattern, which features a meridional tripolar pattern during decaying El Niño summers, with excessive precipitation in central eastern China along the Yangtze River valley (27.5°–32.5°N, 102°–120°E) but drier or even drought conditions in southern (20°–27.5°N, 102°–120°E) and northern (32.5°–45°N, 102°–120°E) China, or vice versa (Huang et al. 2007). This is associated with an anomalous anticyclone over the western North Pacific forced by the SST anomalies there and over the Indian Ocean during decaying El Niño summers (Li et al. 2008; Xie et al. 2009; Wu et al. 2009, 2010). The Silk Road teleconnection, a pattern forced by Indian monsoon heating and characterized by the propagation of a stationary Rossby wave along the Asian jet in the upper troposphere, also affects East Asia, mainly northern China precipitation (Wu et al. 2003; Ding et al. 2011).

Drought trends over China since about 1950 are characterized by a zonal dipole pattern, with an increasing trend over the central part of northern China and a decreasing tendency over northwestern China. The drying and warming trend over northern China is associated with an interdecadal weakening of the East Asian summer monsoon circulation, which has been mainly linked to the 1970s phase transition of the PDO from negative to positive values (Zhou et al. 2009a, 2013). Although the weakening of the monsoon circulation is well reproduced by AMIP-type simulations (Li et al. 2010), the associated anomalous precipitation change found in observations is poorly reproduced over East Asia. This is likely in part due to the biases that exist in simulating the climatological precipitation in this region, resulting from the inability of current relatively coarse global models to resolve the complex terrain over Asia (Zhou et al. 2008a,b; Li et al. 2015).

While CMIP5 experiments indicate that aerosols act to weaken the monsoon circulation, the simulated change is much weaker than observed (Song et al. 2014). A 50–70-yr variation in the PDO index appears to be imprinted in century-scale variations of drought in northern China (Qian and Zhou 2014).

Up to now, most efforts have focused on exploring the predictive skill of East Asian monsoon precipitation, with few examining drought predictability. Previous studies show that climate models have limited skill in simulating and predicting the precipitation in terms of both climatological mean state and interannual variations (Chen et al. 2010; Zhou et al. 2009b). In contrast, the variability of East Asian monsoon circulation is well captured (Zhou et al. 2009c; Song and Zhou 2014a). A successful reproduction of the interannual EASM pattern depends highly on the Indian Ocean–western Pacific anticyclone teleconnection (Kim et al. 2012; Song and Zhou 2014a,b). Finally, Zhang and Zhou (2015) note that in climate change projections, most climate models simulate increasing drought frequency and intensity over East Asia, mainly in southeastern Asia, although the models differ regarding drought patterns and severity.

Figure 7 (right) shows that the link between precipitation over eastern China, Korea, and Japan with SST varies seasonally, with the strongest ties in DJF and MAM; reduced precipitation in the region is tied to La Niña and cold Indian Ocean SST. During JJA the correlation to SST is overall weak. During SON the correlations with precipitation are negative in the western North Pacific and positive in the northern Indian Ocean and the eastern tropical Pacific.

These results are consistent with those of Yang and Lau (2004), who found that MAM precipitation in southeastern China is linked to ENSO; reduced precipitation occurs in years with an abnormally cold central and eastern tropical Pacific and Indian Ocean. Yang and Lau (2004) found that on average in southern China (south of the Yangtze River), MAM and JJA precipitation each account for about 35% of the annual total, with JJA presenting a more complicated picture (see above). They also found that in years with abnormally warm SSTs over the warm pool and northern Indian Ocean and abnormally cold SSTs over the western North Pacific, precipitation over central eastern China tends to be anomalously high (see also Wu et al. 2009, 2010). They further found a tendency for a weakened East Asian monsoon circulation and a delayed monsoon onset in years for which SSTs in the central and eastern tropical Pacific are abnormally warm, resulting in reduced late summer precipitation over northern China.

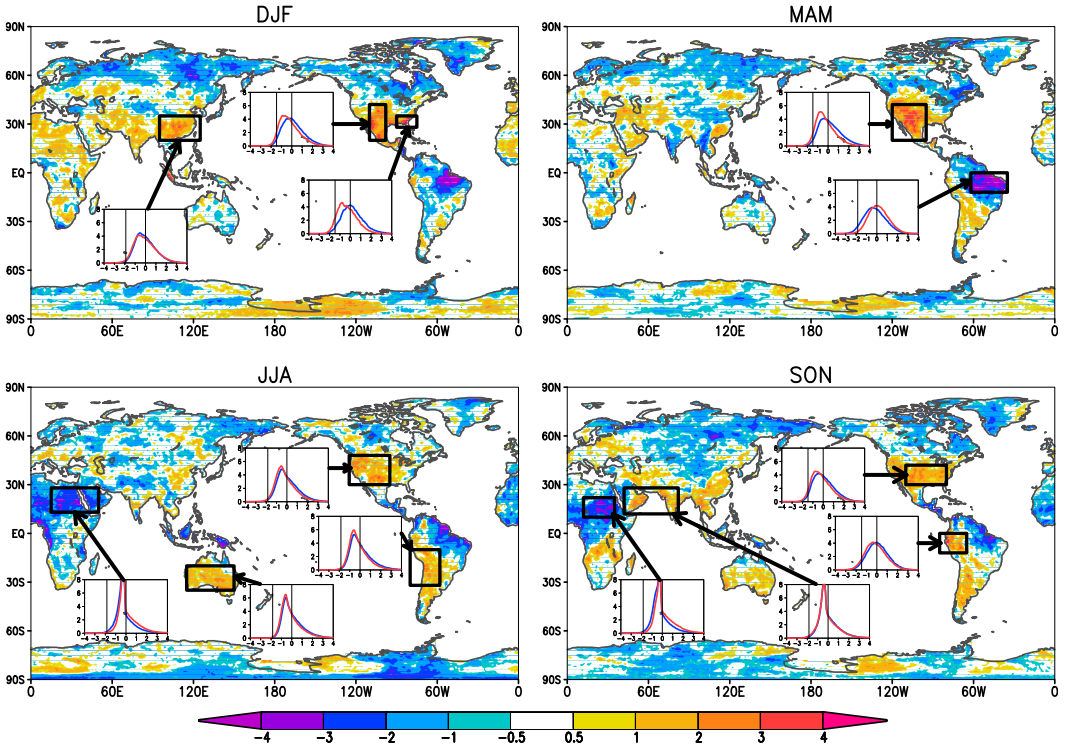

FIG. 10. As in Fig. 2 (top), but for each season.

The above linkages are reflected to some extent in the model results in Fig. 7 (right), although without any evidence of a strong link to SST in the warm pool. Figure 7 features the typical SST anomaly patterns that dominate the East Asian climate during the mature phase of El Niño (boreal winter) extending into the decaying-year summer (Wu et al. 2009). This type of interannual monsoon–SST relationship is well captured by the AMIP simulations of the CMIP3 and CMIP5 models (Song and Zhou 2014a).

A comparison of the observed and model-generated changes in Fig. 3 indicates that the reduced precipitation over southeastern China over the last three decades is linked to SST. Figure 9 shows these long-term changes have occurred primarily during spring and fall, although DJF does show an enhanced probability of extreme dryness (Fig. 10). Figure 11 shows that the warming of the last three decades is associated with an enhanced probability of extreme warm seasons especially during JJA over northwestern China, Korea, and Japan, including most of East Asia during SON.

g. *India*

Kanikicharla et al. (2016, manuscript submitted to *J. Climate*) in their comprehensive review of monsoon droughts over India, note that Indian drought is indeed synonymous with monsoon failure and that a number of historical droughts have led to severe famines and great human and economic losses. They use a century-long time series of Indian summer monsoon rainfall (ISMR) to capture the characteristic spatiotemporal features of deficit monsoons and their possible driving mechanisms. They particularly discuss the low-frequency modulation of ISMR and the associated drought area extent in India with respect to global climate phenomena, and they employ a large suite of AMIP-type model simulations to assess the predictability of Indian drought.

Some key findings from that article include the following:

- Monsoon failures are linked to preceding winter and spring snow accumulation over the Himalayas and larger regions of Eurasia and to the occurrence of warm ENSO events in the Pacific (with the latter link being much stronger).
- The leading EOF of Indian monsoon rainfall has a conspicuous resemblance to the rainfall anomaly pattern associated with major droughts, and that the EOF's time series correlates well with an ENSO-like SST pattern in the Pacific.
- The low-frequency behavior of monsoon rainfall and the drought area index goes hand in hand with the opposite sign of the Niño-3.4 index (which captures

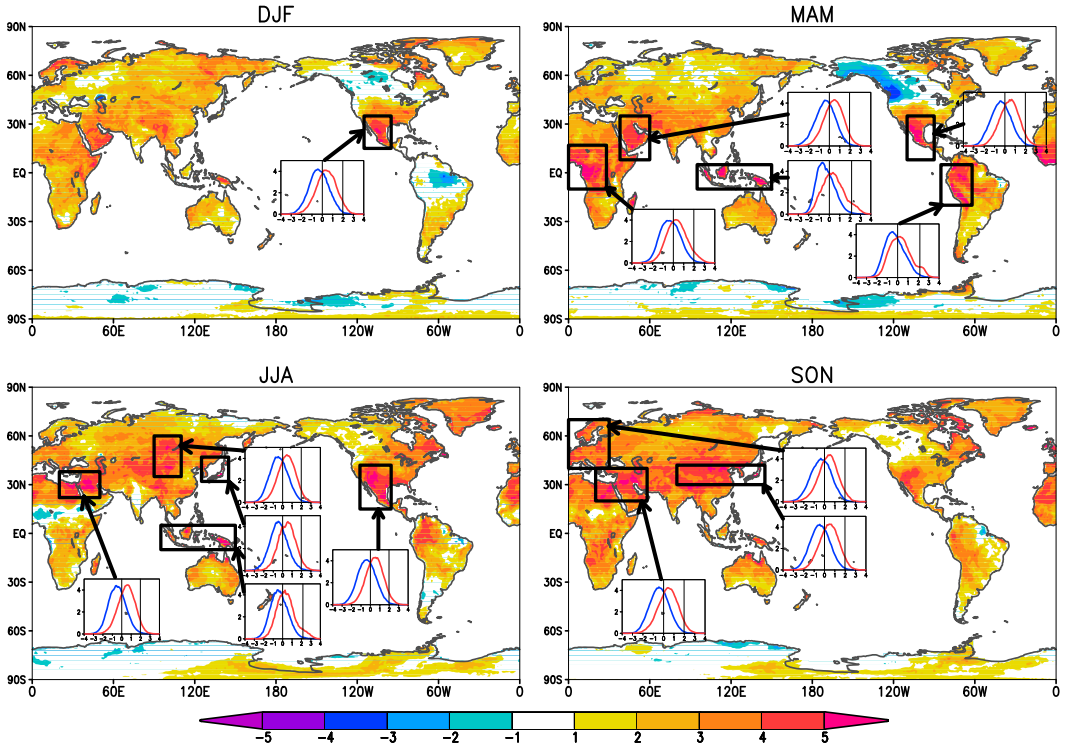

FIG. 11. As in Fig. 2 (bottom), but for each season.

the ENSO and AMO), although with a large difference in their evolution during recent decades. This indicates that the behavior of the Indian monsoon in recent decades cannot be fully explained by known global teleconnections and that other factors (e.g., Indian Ocean variability and aerosols) could be influencing its variability on interannual and decadal time scales (e.g., Ramanathan et al. 2005; Lau et al. 2006; Gautam et al. 2009).

- AGCM simulations forced with global and regional SSTs are able to reproduce the low-frequency variability well, and runs with observed SSTs in the Pacific but with climatological SSTs elsewhere generally produce the sign of many droughts in the past century. The simulated rainfall deficits, however, are much smaller than observed.
- Global warming is probably altering known teleconnections, complicating our ability to predict Indian drought.

These findings emphasize the challenges faced in predicting drought over India and surrounding regions within a changing climate. Figure 1 (top) emphasizes the weak link between annual mean precipitation over southern Asia and global (and in particular ENSO) SST in recent decades, although it also shows (Fig. 1, bottom) that temperature variations in the broader south Asian monsoon region do have strong ties to global SST. Figure 7 (center) highlights the strong seasonality in the simulated link between precipitation and SST in recent decades, with only MAM showing a substantial link to ENSO: El Niño (La Niña) is associated with reduced (enhanced) precipitation. [This link is consistent with observations and robust across the models (Fig. B3).] ENSO may provide important preconditioning of the land (e.g., soil moisture and snow) during the premonsoon months, so that the role played by SST in monsoon droughts, while important, may be indirect. We note that such effects may be missed by contemporaneous correlations, as in the present analyses.

h. Australia and the Maritime Continent

As reviewed in Cai et al. (2014), the influence of climate variability and change on Australia is complex and varies both regionally and seasonally. In particular, they indicate how the continent is impacted by the IOD, the southern annular mode (SAM), and ENSO, as well as the poleward edge of the Southern Hemisphere Hadley cell.

The corresponding correlation map in Fig. 1 (top) shows aspects of a negative IOD, La Niña, and a negative PDO. Consistent with the discussion in Cai et al. (2014), the key SST forcing regions driving Australian precipitation appear to be the tropical Pacific just west

of the date line and areas in the eastern Indian Ocean just to the north and west of Australia. This is highlighted in Fig. 8 (left), with spring (SON) and summer (DJF) showing the strongest relationship between Australian precipitation and remote SST. In summer, the pan-Australian rainfall is dominated by contributions from northern and eastern Australia; as such, dry conditions are associated with both a warm central tropical Pacific (with weaker correlations extending eastward across the Pacific), that is, an El Niño, and a warm Indian Ocean SST (basin-wide warming that usually accompanies an El Niño). During the spring, the contributions to the pan-Australian rainfall come about equally from northern and southern Australia, and ENSO and the IOD have the highest coherence to rainfall in those regions. As such, spring appears to have the strongest (spatially most coherent) link to ENSO, with dry conditions linked to El Niño and a cool anomaly in the eastern Indian Ocean. [This result is robust across models and observations (Fig. B4).] In contrast, during fall (MAM) and particularly during winter (JJA), the pan-Australian precipitation comes mostly from southern Australia. The deficit during fall (MAM) shows the greatest link with cold SST anomalies to the northwest, while the deficit during winter (JJA) is linked to cold SST anomalies in the eastern Indian Ocean associated with the development phase of a positive IOD. These cold SST anomalies are unfavorable for weather systems that typically deliver rain-producing moisture over southern Australia.

Recently, Australia experienced one of its most severe, recorded droughts: the Millennium Drought, which lasted about 10 years (2000–09). Cai et al. (2014) showed that the associated precipitation anomalies had substantial seasonal variation, with austral summer [December–March (DJFM)] showing positive precipitation anomalies in northwestern Australia and with some of the largest deficits over other parts of Australia occurring during late fall and winter. Figure 3 shows that the annual mean differences (1998–2011 minus 1979–93) largely reflect the summer precipitation increases in northwestern Australia during that drought. The relevant seasonality is well captured by the models (Fig. 9), which show the northern Australian precipitation surfeits in the recent 14-yr period during DJFM and the deficits associated with the Millennium Drought during April–July [AMJJ; cf. Fig. 3 in Cai et al. (2014)]. Much of Australia in fact experienced an increased risk of dry winters (JJA) over the last 14 years (Fig. 10).

Cai et al. (2014) show that the precipitation deficits over southwestern Western Australia partly result from a long-term upward trend in the SAM; this trend accounts for half of the winter rainfall reduction there. For southeastern Australia, CMIP5 model simulations indicate only weak trends in the pertinent climate modes, apparently underestimating the observed poleward expansion of the subtropical dry zone and associated impacts. They conclude that ''although climate models generally suggest that Australia's Millennium Drought was mostly due to multidecadal variability, some late-twentieth-century changes in climate modes that influence regional rainfall are partially attributable to anthropogenic greenhouse warming.''

The Maritime Continent is strongly affected by ENSO during JJA and SON (Fig. 8, right); El Niño conditions lead to reduced precipitation. JJA also exhibits positive correlations with tropical and North Atlantic SST. In contrast, DJF and MAM precipitation observations show little connection with ENSO, and the overall correlations with SST are weak: weak negative correlations with SST in the central tropical Pacific, and, for MAM, weak positive correlations with local SST. Chang et al. (2003), however, point out that the low correlations between Indonesian rainfall and ENSO during the Northern Hemisphere winter monsoon period are partly due to the spatial averaging of the rainfall in two regions with opposite characteristics.

i. Europe and the Mediterranean region

Here, we review the primary modes of variability that affect the European and Mediterranean climate on subseasonal-to-interannual and longer time scales, with a focus on their impacts on precipitation and/or surface temperature fields. We shall see that northern and central European meteorological drought drivers and impacts are often different or even opposite to those for southern Europe and the Mediterranean region.[9] In addition, we will discuss reported trends in meteorological drought in Europe and projected drought changes in Europe with increasing greenhouse gases.

Correlations of the NAO and the AMO with drought occurrence in Europe have been documented, and the effects of other modes of variability including ENSO have been postulated (see below). Nonetheless, these relationships do not seem to be associated with the high interannual predictability of meteorological drought in central and northern Europe (Dutra et al. 2014). Overall SST anomalies, which may be associated with large-scale modes of variability, explain only a small fraction of the annual mean variability in precipitation (less than 10%) and temperature (less than 20%) over Europe

[9] In this section, the term Mediterranean is used to indicate areas surrounding the sea from southern Europe, northern Africa, and the Middle East; the term Europe indicates northern and central Europe.

(see Fig. 1). Hence, the predictability associated with large-scale modes of variability that have been linked to drought occurrence in Europe is still unclear from the existing literature. In addition, it has been highlighted that the circulation patterns and weather types related to the most severe droughts in Europe often vary across seasons and regions (Stahl 2001, see also below; Fleig et al. 2011).

Hurrell (1995) showed that during high NAO index winters (such as those that occurred in 1983, 1989, and 1990), the axis of maximum moisture transport shifts to a more southwest–northeast orientation across the Atlantic and extends much farther north and east onto northern Europe and Scandinavia, accompanied by a reduction in moisture transport over southern Europe, the Mediterranean, and northern Africa. As a result, northern Europe is mild and wet during the positive phase of the NAO and cold and dry during the negative phase, whereas the reverse is true for southern Europe and most of the Mediterranean but with the Levant also being wet (dry) during a positive (negative) NAO (e.g., Xoplaki et al. 2004). In recent decades the NAO index has shown a return toward more negative values, although with a marked increase in year-to-year winter variability (Hanna et al. 2015).

The summer NAO (sNAO) has a more northerly location and smaller spatial scale than its winter counterpart (Folland et al. 2009). Nevertheless, the sNAO has a strong influence on northern European rainfall, temperature, and cloudiness through changes in the position of the North Atlantic storm track, thus playing an important role in generating summer climate extremes, including flooding, drought, and heat waves in northwestern Europe. A positive sNAO also results in wetter conditions in the central/eastern part of the Mediterranean.

Folland et al. (2009) further suggest that on interdecadal time scales, sNAO variations are partly related to the AMO. While the exact link between the two is still unclear, Sutton and Dong (2012) show that, during the 1990s, European climate shifted toward a pattern characterized by anomalously wet summers in northern Europe and hot, dry, summers in southern Europe, with related shifts in spring and autumn, and they point to recent evidence suggesting that the warming was largely caused by an acceleration of the Atlantic meridional overturning circulation (AMOC) and associated northward ocean heat transport in response to the persistent positive phase of the winter NAO in the 1980s and early 1990s (Robson et al. 2012). However, uncertainties still exist regarding the processes underpinning AMO variability; for example, the role of anthropogenic aerosols (Booth et al. 2012). Mariotti and Dell'Aquila (2012) show that decadal variability associated with the NAO, the sNAO, and the AMO significantly contribute to decadal climate anomalies over the Mediterranean region. The positive phase of the AMO is associated with warmer than usual decades especially in summer, whereas the AMO has no influence on Mediterranean winter temperatures. Land–atmosphere feedbacks also play a role in shaping the observed decadal variability, enhancing the large-scale influences. Della Marta et al. (2007) found a relationship between western Mediterranean heat waves and the AMO. On decadal time scales, the AMO and NAO explain over 60% of the observed area-averaged summer temperature and winter precipitation variability, respectively (Mariotti and Dell'Aquila 2012).

The Mediterranean region displays a robust drying trend in both precipitation and the land water balance since the 1950s (Sheffield et al. 2012; Hartmann et al. 2013; Greve et al. 2014), a signal consistent with climate change projections (see below). Nonetheless, a possible attribution of these historical trends to increased greenhouse gas concentrations has not been provided so far, and it is possible that decadal variability associated with large-scale modes of variability could have played a role. Hoerling et al. (2012) note that for the land area surrounding the Mediterranean Sea, 10 of the 12 driest winters since 1902 occurred in just the last 20 years, and they propose that the drying over the last century can be understood as a response to a uniform global ocean warming and to modest changes in the oceans' zonal and meridional SST gradients, with warming in the Indian Ocean producing an enhanced drying signal attributable to an atmospheric circulation response resembling the positive phase of the NAO. Kelley et al. (2012), in a combined observational and modeling analysis, argue that while the upward NAO trend over recent decades can explain much of the concurrent Mediterranean region drying, it cannot explain drying in the Levant, which they instead argued was consistent with drying in response to rising greenhouse gases.

With respect to climate change projections, the Mediterranean shows one of the most robust responses (across models) to greenhouse gas increases over the twenty-first century (Giorgi and Lionello 2008; Seneviratne et al. 2012a; Orlowsky and Seneviratne 2013). Projected changes, which reinforce trends already observed during the twentieth century, include both a reduction in precipitation and an increase in evapotranspiration (because of increased incoming radiation and higher air temperature), with associated soil moisture reductions (e.g., Mariotti et al. 2008; Orlowsky and Seneviratne 2012, 2013; Seager et al. 2014b; Mariotti et al. 2015).

Uncertainties remain in our understanding of the NAO's link to SST changes (Bretherton and Battisti

2000) and of its link to global warming (Gillett et al. 2003), its connection to the Arctic Oscillation (AO; Ambaum et al. 2001), its link to the stratosphere (Scaife et al. 2005), and its possible modulation by ENSO (Brönnimann 2007) and other modes of variability such as the Scandinavian (SCA) and East Atlantic (EA) patterns (e.g., Comas-Bru and McDermott 2014). In fact, SCA, EA, and the East Atlantic/Western Russia (EAWR) patterns (Barnston and Livezey 1987) have also been suggested to contribute substantially to European climate variability (e.g., Bueh and Nakamura 2007; Iglesias et al. 2014; Ionita 2014).

A number of studies have produced objectively defined drought catalogs for Europe (Lloyd-Hughes et al. 2010; Spinoni et al. 2015). Parry et al. (2010) also produced summaries of the major large-scale European droughts of the last 50 years based on the catalog compiled by Lloyd-Hughes et al. (2010). As summarized in Stahl (2001), major droughts over the period 1960–90 occurred during 1962–64, 1972–76, 1983, and 1989/90. They note that ''Most of the severe summer droughts across Europe were associated with high pressure systems across central Europe. Generally, drought associated synoptic meteorology is characterized by high mean sea level pressure (MSLP), but the circulation pattern types vary not only with the season but also for all individual discussed events.''

Figures 2b and 11 show that there has been a pronounced shift in the probability of extremely warm years over the last three decades over most of Europe, with the shift equal to more than 1.5 times the climatological probability of 2.5% over many regions. This shift, most pronounced during fall, appears to be associated with a shift in the mean temperature over the recent decades, which is likely attributable in part to enhanced greenhouse gas forcing (Bindoff et al. 2013). Figures 2a and 10 show that changes in precipitation over the last three decades are generally small, although there is a general tendency for a greater probability of extremely dry years throughout central and southern Europe. This appears to hold for each season as well. This result is also robust when investigating longer-term trends since the 1950s, either for precipitation or precipitation minus evapotranspiration (Seneviratne et al. 2012a; Hartmann et al. 2013; Greve et al. 2014).

While the present review and special issue focus on meteorological (i.e., precipitation based) drought and its relation to SSTs as a driver, we note the following additional points regarding drought drivers in Europe:

- In general, agricultural (soil moisture) and hydrological (streamflow) drought events in Europe are caused by a prolonged deficit in precipitation (Tallaksen et al. 2015; Stagge et al. 2015). However, in central Europe, evapotranspiration is an important driver for soil moisture droughts, in some cases to the same degree as precipitation (e.g., Seneviratne et al. 2012b; Teuling et al. 2013). In addition, in cold climates, temperature anomalies also play a role in the development of hydrological drought (Van Loon and Van Lanen 2012).
- Prior storage deficits in the form of soil moisture, snow, and groundwater are important for the occurrence and development of soil moisture and streamflow droughts (Van Loon and Van Lanen 2012; Orth and Seneviratne 2013; Staudinger et al. 2014; Tallaksen et al. 2015). They thus provide some essential sources of drought predictability, in particular given the low SST control on interannual precipitation variability in Europe (Fig. 1).

j. Northern Eurasia

Figure 1 shows that across the vast expanse of northern Eurasia, neither precipitation nor temperature is strongly affected by SST on interannual time scales. Schubert et al. (2014), in examining both heat waves and drought over northern Eurasia, highlighted the central role of anticyclones in the region; these act to warm and dry the atmosphere and land surface over many important agricultural regions from European Russia to Kazakhstan and beyond. They discuss how the development of anticyclones is linked to different air masses, especially the intrusion of Arctic air masses that occasionally combine with subtropical air (e.g., associated with the Azores high in eastern Europe and western Russia) to produce especially severe drought and heat wave events. Schubert et al. (2014) found that some of the most severe summer heat waves are linked to distinct Rossby wave trains spanning the continent that, while producing severe heat in one location, cause a juxtaposition of wet and cool conditions in regions thousands of kilometers to the east or west—a phenomenon noted more than 100 years ago in early descriptions of northern Eurasian heat waves.

Given the lack of a strong SST connection, the predictability of the most severe events in northern Eurasia is limited to the time scales of the internally forced Rossby waves (typically less than 1 month), although some aspects of heat waves appear to be predictable for several months: the surface temperature anomalies at the center of the heat wave associated with soil moisture anomalies that persist through the summer. Schubert et al. (2014), using an AGCM experiment in which soil moisture feedbacks were disabled, showed that temperature variability is strongly tied to soil moisture variability particularly in the southern parts of northern Eurasia extending from southern Europe eastward across the Caucasus, Kazakhstan, Mongolia, and northern China.

They note that longer-term droughts (lasting multiple years) do occur but are largely confined to the southern parts of northern Eurasia, where there appears to be a weak link to SST and an important control from soil moisture.

Schubert et al. (2014) further showed that the observed warming over northern Eurasia in the last three decades is part of a large-scale warming pattern with local maxima over European Russia and over Mongolia–eastern Siberia (see also Fig. 3). Precipitation changes consist of deficits across Eurasia covering parts of northeastern Europe, European Russia, Kazakhstan, southeastern Siberia, Mongolia, and northern China and increases across Siberia poleward of about 60°N. Comparisons of these changes with Fig. 3, however, indicate some sensitivity of the computed changes to the years chosen for averaging. Model simulations carried out with idealized versions of the observed SST anomalies indicate that the changes over the last three decades are consistent with a global-scale response to PDO-like and AMO-like SST patterns, intensified by a global warming SST trend.

Figure 2 indicates that any changes in the probability of heat waves are likely a consequence of an overall warming trend that affects much of Eurasia (although more strongly in the southern regions). In particular, the increase in the probability of extreme heat largely results from an overall shift in the pdf of temperature (a change in the mean) rather than from a change in its shape. Schubert et al. (2014) point to studies indicating an enhanced probability of heat waves across northern Eurasia by the second half of the twenty-first century. Existing studies and analyses of climate change projections of the Coupled Model Intercomparison Project (CMIP), however, show less certainty regarding future drought (e.g., Seneviratne et al. 2012a; Orlowsky and Seneviratne 2013), reflecting the greater uncertainty of precipitation and soil moisture projections.

4. Concluding remarks

The results presented here, and in the regionally focused articles that make up this special collection, illustrate that considerable progress has been made in our understanding of the occurrence and predictability of meteorological drought in different parts of the world. The importance of large-scale teleconnections, whether they are linked to ENSO or other SST variability or whether they consist of large-scale atmospheric circulation anomalies that are unforced by SST (internal to the atmosphere), is now well established. As such, in addressing the causes and predictability of meteorological drought for any particular region of the world, we have to address the following questions: 1) what are the large-scale drivers (if any) of precipitation deficits relevant to that region, and 2) what are the unique climatological features of that region that act to enhance or suppress the large-scale precipitation tendencies?

Although the individual articles in this special collection have in many cases provided answers to both of these questions (as we have attempted to summarize in section 3), this article goes further by providing a more global perspective on these two questions within the context of the ''consensus'' view provided by the simulations with current state-of-the-art AGCMs forced by observed SST.

In particular, we have provided our current best estimate of regions where SST forcing provides some control on annual precipitation and temperature variability. This is critically important to the drought prediction problem, since the regions where SST does play a substantial role in driving precipitation (and temperature) variability are also the regions where we can expect to have some degree of predictability on seasonal and longer time scales. We have also underscored the importance of ENSO (tropical Pacific SST) in providing that potential predictability in many parts of the world (including the Americas, eastern and southwest Asia, Australia, and the Maritime Continent), although not exclusively so, with other ocean basins also playing a role in some regions of the world, either individually or in concert with ENSO. These include the Indian Ocean (the Indian Ocean dipole affecting Australia and the Indian Ocean basin mode affecting East Asia), the Atlantic Ocean (affecting northern South America, parts of the southern and eastern United States, and the Sahel), and the Mediterranean Sea (affecting southern Europe and northern Africa), although the extent to which some of these SST patterns are independent of ENSO is still not fully resolved.

A number of regions dominated by monsoonal climates have droughts that are intimately tied to failures in the development of monsoonal rains. The GDIS articles highlight the substantial progress made in identifying the sources of these failures. From a global perspective, ENSO significantly affects much of the Asian–Australian monsoon system. On decadal time scales, the apparent weakening of the global land monsoon since the 1950s has been linked to the interdecadal Pacific oscillation as well as to a warming trend over the central eastern Pacific and the western tropical Indian Ocean and also to anthropogenic aerosol forcing. Much remains to be understood, however, about the observed trends in monsoonal precipitation.

Northern Eurasia, central Europe, and central and eastern Canada stand out as regions with little SST-forced impacts on precipitation on interannual time

scales. This has important implications for the predictability and the time scales of droughts in these regions. In northern Eurasia, for example, droughts and heat waves are predominantly linked to the development of anticyclones and, although extreme, they rarely last longer than one season. In central Europe a number of different atmospheric teleconnections that are unforced (or only weakly forced) by SST do appear to play a role, although these are relatively short lived and have little predictability on seasonal and longer time scales: here, evapotranspiration is an important driver for soil moisture droughts, and predictability on longer time scales is tied to soil moisture memory and feedbacks.

Although the annual mean results provide a broad picture of the role of SST, our results also highlight the strong seasonality in the link to the SST that occurs in most regions of the world. As such, the timing and duration of drought has as much to do with the seasonality of the link to SST as it has to do with the time of year that local climatological (land and circulation) conditions make a region most prone to drought. East Africa is an example of a particularly challenging region in which to model and understand drought, because of the heterogeneous local rainfall regimes that include unimodal and bimodal annual cycles combined with strong seasonality in the response to ENSO.

We have also addressed longer-term (decadal) meteorological drought and the link to SST. In particular, we present a remarkable example of the ability of current climate models (when forced with observed SST) to reproduce the long-term changes in precipitation and surface temperature that have occurred over the last three decades. The model results show that the shifts to drought or pluvial conditions (and warming) have a global coherence driven by long-term SST changes (a combination of the PDO, AMO, and a long-term trend). Our analysis of the most extreme seasonal and annual mean precipitation deficits shows that the associated changes in the tails of the probability density functions (pdfs) in most regions of the world reflect overall shifts in the mean rather than changes in the shape of the pdfs (although this may not be true for northeastern South America, a region exhibiting a substantial decrease in the probability of extremely dry years over the last three decades but with little change in the probability of extreme wet years). The success of the models in reproducing the observed changes provides the basis for further research to dissect the causes of these changes and address their potential predictability.

One consequence of the decadal and longer-term variations is that a number of regions exhibit substantial nonstationarity in the relationships between SST and precipitation on interannual time scales (examples where this is particularly evident include West Africa and India), complicating our ability to understand these relationships and take advantage of them for prediction. Global warming, while not a focus of this article, is clearly an important issue when addressing longer-term changes in drought. In fact, as discussed in a number of the articles in this special collection, some regions of the world appear to already be seeing the impacts of warming on drought (e.g., the southwestern United States, the Mediterranean region, and central Europe), although much work needs to be done to better understand the relative contributions of decadal SST variability and long-term SST trends to drought.

Finally, we must emphasize that current climate models, including the AGCMs used here, are far from perfect. A key factor emphasized in many of the contributing articles and further highlighted here is the challenge of reproducing some of the complex local precipitation regimes (including the annual cycle) that must be simulated correctly in order to properly simulate the impact of large-scale forcing on regional drought. The relatively coarse resolution of current climate models hinders that process, and so we can at best obtain a spatially averaged picture or in some cases even an incorrect assessment of the impacts. Examples where this is especially critical include East Africa and East Asia, regions that are characterized by complex terrain and highly heterogeneous regional precipitation regimes. We should note that this situation will likely improve in the coming years as it becomes feasible to apply ultrahigh resolution ($<$10 km) global models to climate problems. However, not all problems concerning the simulation of important teleconnections can be blamed on insufficient resolution. For example, deficiencies in the simulation of the atmospheric response to equatorial Atlantic SSTs and the link to West African drought are likely tied to deficiencies in the simulation of the climatological mean state. Furthermore, considerable work still needs to be done to improve our coupled atmosphere–ocean general circulation models that still have, for example, great difficulties in correctly reproducing the seasonal cycle and variability of tropical Atlantic SST.

How do we move forward? Drought is an immensely complex problem that must be attacked on many fronts by researchers from around the world, with well-considered links to users who may benefit from the research. GDIS is an ongoing activity that supports this cause. GDIS will continue to encourage researchers and users around the world to work together to improve systematically our understanding of, prediction of, and adaptation to drought, for example, by facilitating the development of improved models and long-term

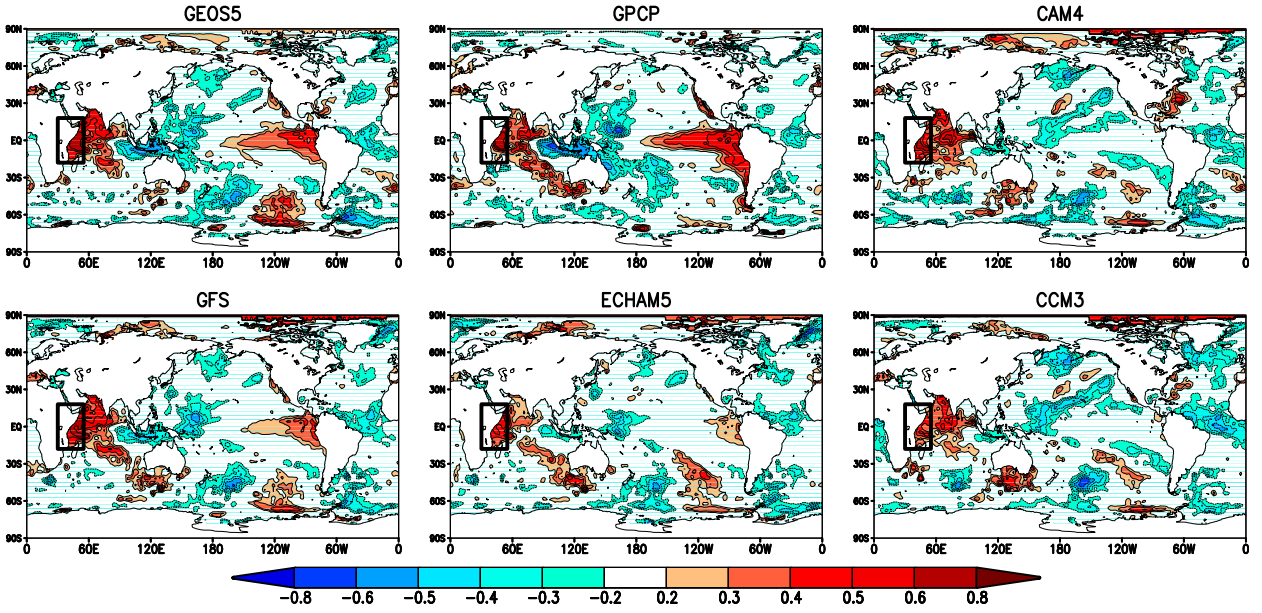

FIG. B1. The correlations between the ensemble mean precipitation over East Africa and SST for each model during SON (1979–2011). (top center) Also shown is the correlation based on GPCP observations.

consistent drought-specific observations, and providing global access to data portals that summarize our ever-evolving knowledge on the subject.

Acknowledgments. The various contributions to this paper were made possible by the support of the host organizations of the coauthors, as noted in the acknowledgments of the contributing Global Drought Information System (GDIS) special collection papers. The GDIS effort is sponsored and supported by the World Climate Research Programme (WCRP: CLIVAR and GEWEX) and various partner organizations

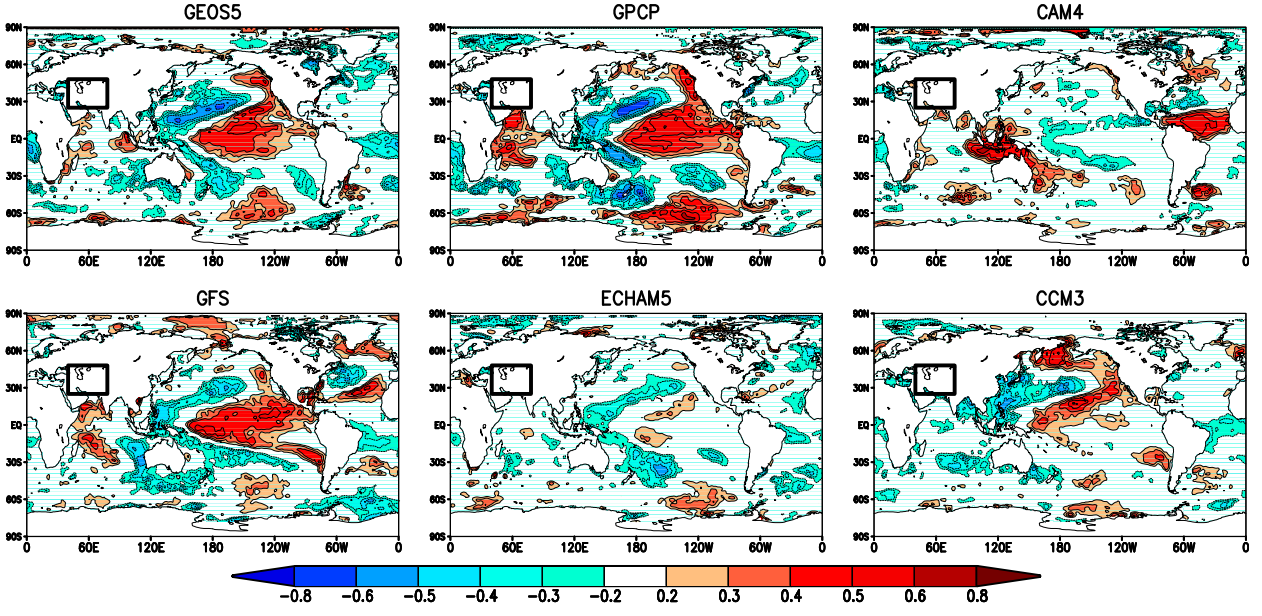

FIG. B2. The correlations between the ensemble mean annual precipitation over the Middle East and SST for each model (1979–2011). (top center) Also shown is the correlation based on GPCP observations. We note that there is some sensitivity to the region chosen for some of the models (e.g., the results for CCM3 looks more like those of the other models and observations if the region is truncated on the southern and eastern edges).

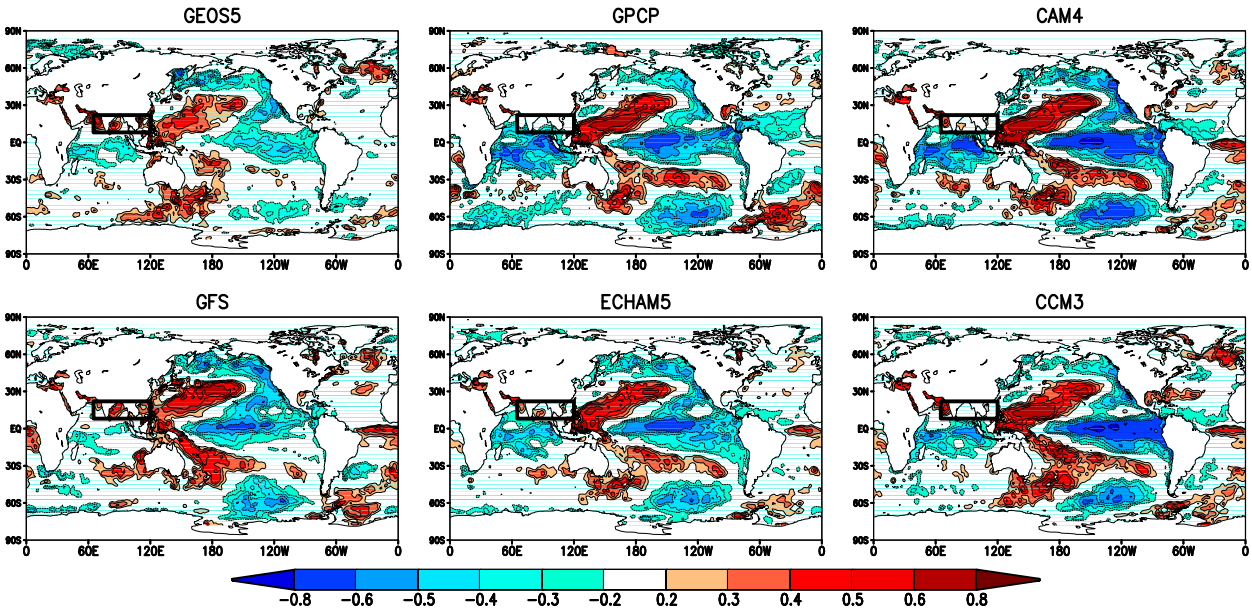

FIG. B3. The correlations between the ensemble mean precipitation over southern Asia and SST for each model for MAM (1979–2011). (top center) Also shown is the correlation based on GPCP observations.

including the National Oceanic and Atmospheric Administration (NOAA), the National Aeronautics and Space Administration (NASA), the National Integrated Drought Information System (NIDIS), the World Meteorological Organization (WMO), the U.S. CLIVAR program, the Group on Earth Observations (GEO), the European Commission Joint Research Centre (JRC), the National Science Foundation (NSF), and the European Space Agency (ESA)–European Space Research Institute (ESRIN). Support for the overall development of this synthesis article was provided by NASA's Modeling, Analysis and Prediction Program. The GLDAS-2 data used in this study were acquired as part of the mission of NASA's Earth Science Division and archived and distributed by the Goddard Earth Sciences (GES) Data and Information Services Center (DISC).

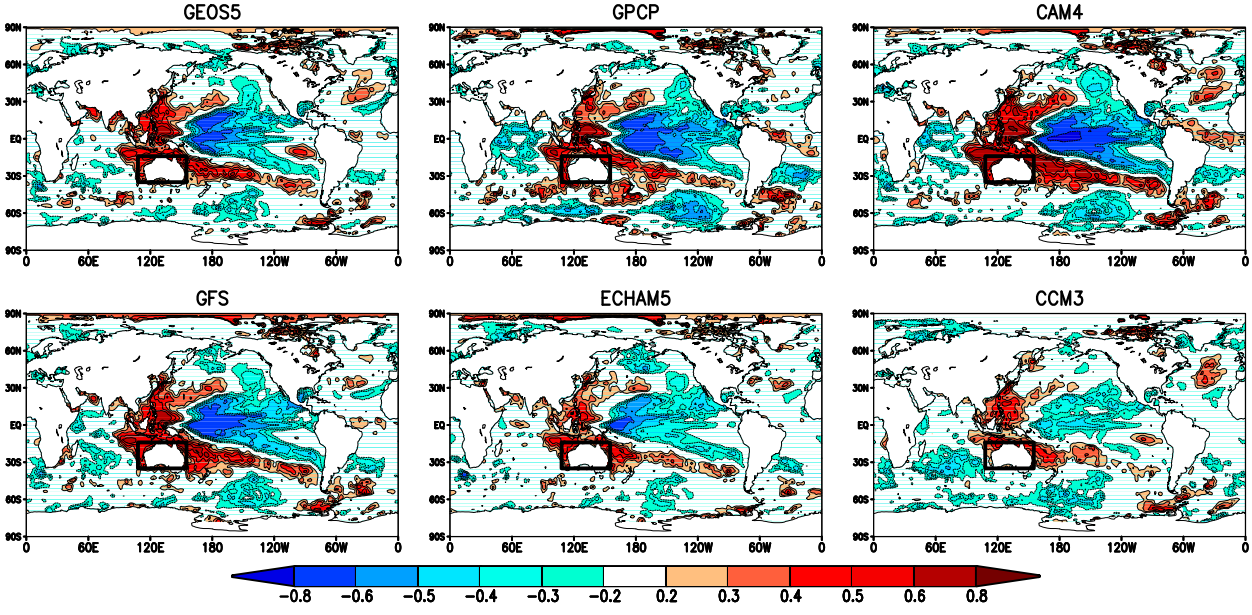

FIG. B4. The correlations between the ensemble mean precipitation over Australia and SST for each model for SON (1979–2011). (top center) Also shown is the correlation based on GPCP observations.

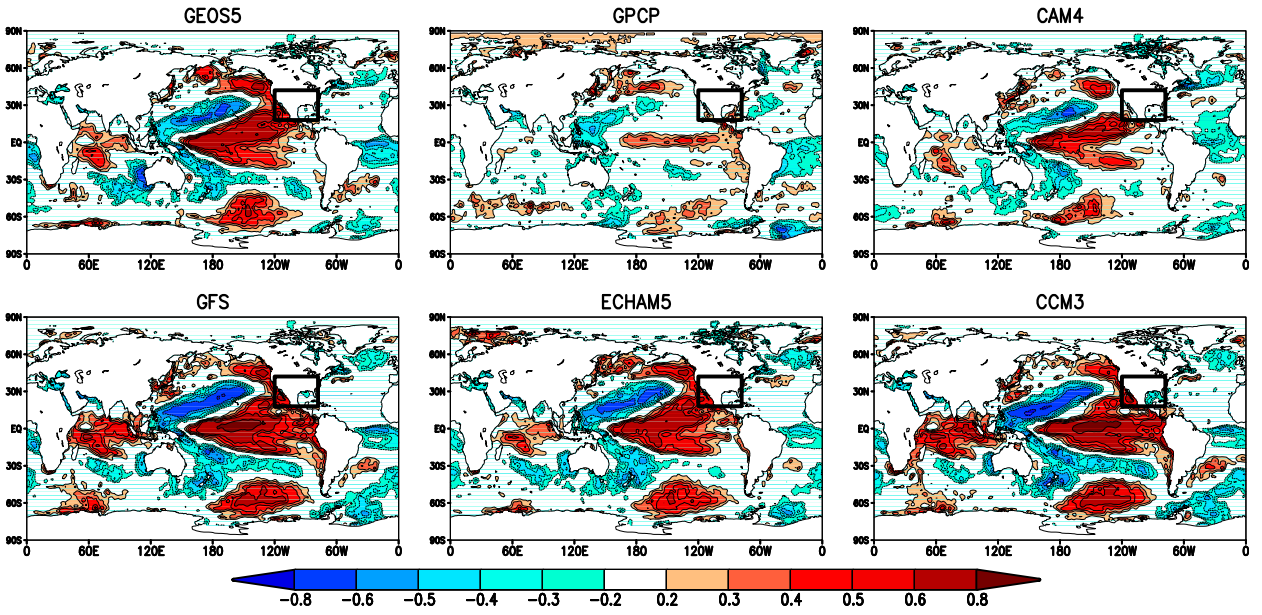

FIG. B5. The correlations between the ensemble mean precipitation over the United States and northern Mexico and SST for each model for MAM (1979–2011). (top center) Also shown is the correlation based on GPCP observations.

APPENDIX A

Description of the Models and Experiments

Many of the results presented in this paper are based on Atmospheric Model Intercomparison Project (AMIP)-style simulations produced with five different atmospheric general circulation models (AGCMs). The models used are GEOS-5, CCM3, CAM4, GFS, and ECHAM5. The years 1979–2011 were subsetted from 12 of each model's ensemble members, providing a dataset of sixty 33-yr simulations. The following provides a brief description of the models and the experiments.

The NASA Goddard Earth Observing System, version 5 (GEOS-5), AGCM is described by Rienecker et al. (2008), and an overview of the model's performance is provided by Molod et al. (2012). For these experiments, the model was run with 72 hybrid sigma vertical levels extending to 0.01 hPa and with a 1° horizontal resolution on a latitude–longitude grid. The simulations consist of 12 ensemble members, each forced with observed monthly SST, sea ice, and time-varying greenhouse gases for the period from 1871 to the present. See Schubert et al. (2014) for further details.

A 16-member ensemble covering the period from January 1856 to April 2014 was produced with the NCAR Community Climate Model, version 3 (CCM3; Kiehl et al. 1998). The model was run at spectral T42 resolution with 18 vertical levels. Sea ice was held at climatological values, and SST forcing in the years of interest here combined the Kaplan et al. (1998) SST dataset in the tropical Pacific Ocean (20°N–20°S) with the Hadley Centre SST dataset (Rayner et al. 2003) outside of the tropical Pacific.

A 20-member ensemble covering the period from January 1979 to April 2014 was produced with the NCAR Community Atmosphere Model, version 4 (CAM4), forced by SST and sea ice from the Hurrell et al. (2008) dataset and with time-varying GHGs from the representative concentration pathway 6.0 (RCP6.0) scenario after 2005. The resolution used was $0.94° \times 1.25°$, with 26 vertical levels.

NOAA's Earth System Research Laboratory produced a 50-member ensemble spanning from January 1979 to April 2014 using the NCEP Global Forecast System (GFS; the atmosphere component of the Climate Forecast System) version 2 model (denoted here as ESRL GFSv2). The model was run at spectral T126 resolution with 64 vertical levels and was forced by observed SST and sea ice from the Hurrell et al. (2008) dataset. CO_2 varied with time, but other GHGs were held fixed.

A 20-member ensemble spanning from January 1979 through April 2014 was produced with the ECHAM5 model (Roeckner et al. 2003) forced by the Hurrell et al. (2008) SST and sea ice data, as recommended for use in CMIP5 simulations. These simulations used time-varying GHGs, following the RCP6.0 scenario after 2005, and they used a spectral T159 resolution, with 31 vertical levels.

APPENDIX B

Selected Individual Model Results

Here, we present a few comparisons of the results for individual models and observations, highlighting regions where it is especially important to assess the model dependence of the results (see the text above). While the comparison with observations provides a rough idea of consistency with nature, it must be kept in mind that the observations represent a single realization of nature and thus should differ from the ensemble means of the model runs, which specifically isolate the impact of SST and other forcings, which is our focus here. A careful assessment of the veracity of the models, which is beyond the scope of this paper, would in principle involve determining if a correlation produced for the observations lies within the spread produced by the given model's individual ensemble members. See Figs. B1–B5 for model comparisons.

REFERENCES

Ambaum, M. H. P., B. J. Hoskins, and D. B. Stephenson, 2001: Arctic Oscillation or North Atlantic Oscillation? *J. Climate*, **14**, 3495–3507, doi:10.1175/1520-0442(2001)014<3495:AOONAO>2.0.CO;2.

Barlow, M., B. Zaitchik, S. Paz, E. Black, J. Evans, and A. Hoell, 2016: A review of drought in the Middle East and southwest Asia. *J. Climate*, doi:10.1175/JCLI-D-13-00692.1, in press.

Barnston, A. G., and R. E. Livezey, 1987: Classification, seasonality and persistence of low-frequency atmospheric circulation patterns. *Mon. Wea. Rev.*, **115**, 1083–1126, doi:10.1175/1520-0493(1987)115<1083:CSAPOL>2.0.CO;2.

Barreiro, M., and N. Diaz, 2011: Land–atmosphere coupling in El Niño influence over South America. *Atmos. Sci. Lett.*, **12**, 351–355, doi:10.1002/asl.348.

Bindoff, N. L., and Coauthors, 2013: Detection and attribution of climate change: From global to regional. *Climate Change 2013: The Physical Science Basis*, T. F. Stocker et al., Eds., Cambridge University Press, 867–952.

Booth, B. B. B., N. J. Dunstone, P. R. Halloran, T. Andrews, and N. Bellouin, 2012: Aerosols implicated as a prime driver of twentieth-century North Atlantic climate variability. *Nature*, **484**, 228–232, doi:10.1038/nature10946.

Bretherton, C. S., and D. S. Battisti, 2000: An interpretation of the results from atmospheric general circulation models forced by the time history of the observed sea surface temperature distribution. *Geophys. Res. Lett.*, **27**, 767–770, doi:10.1029/1999GL010910.

Brönnimann, S., 2007: Impact of El Niño–Southern Oscillation on European climate. *Rev. Geophys.*, **45**, RG3003, doi:10.1029/2006RG000199.

Bueh, C., and H. Nakamura, 2007: Scandinavian pattern and its climatic impact. *Quart. J. Roy. Meteor. Soc.*, **133**, 2117–2131, doi:10.1002/qj.173.

Cai, W., A. Purich, T. Cowan, P. Van Rensch, and E. Weller, 2014: Did climate change–induced rainfall trends contribute to the Australian Millennium Drought? *J. Climate*, **27**, 3145–3168, doi:10.1175/JCLI-D-13-00322.1.

Cazes-Boezio, G., A. W. Robertson, and C. R. Mechoso, 2003: Seasonal dependence of ENSO teleconnections over South America and relationships with precipitation in Uruguay. *J. Climate*, **16**, 1159–1176, doi:10.1175/1520-0442(2003)16<1159:SDOETO>2.0.CO;2.

Chang, P., R. Saravanan, and L. Ji, 2003: Tropical Atlantic seasonal predictability: The roles of El Niño remote influence and thermodynamic air–sea feedback. *Geophys. Res. Lett.*, **30**, 1501, doi:10.1029/2002GL016119.

Chen, H., T. Zhou, R. B. Neale, X. Wu, and G. Zhang, 2010: Performance of the new NCAR CAM3.5 in East Asian summer monsoon simulations: Sensitivity to modifications of the convection scheme. *J. Climate*, **23**, 3657–3675, doi:10.1175/2010JCLI3022.1.

Comas-Bru, L., and F. McDermott, 2014: Impacts of the EA and SCA patterns on the European twentieth century NAO–winter climate relationship. *Quart. J. Roy. Meteor. Soc.*, **140**, 354–363, doi:10.1002/qj.2158.

Cook, B. I., J. E. Smerdon, R. Seager, and S. Coats, 2014: Global warming and 21st century drying. *Climate Dyn.*, **43**, 2607–2627, doi:10.1007/s00382-014-2075-y.

——, T. R. Ault, and J. E. Smerdon, 2015: Unprecedented 21st-century drought risk in the American Southwest and central plains. *Sci. Adv.*, **1**, e1400082, doi:10.1126/sciadv.1400082.

Dai, A., K. E. Trenberth, and T. Qian, 2004: A global dataset of Palmer drought severity index for 1870–2002: Relationship with soil moisture and effects of surface warming. *J. Hydrometeor.*, **5**, 1117–1130, doi:10.1175/JHM-386.1.

Della-Marta, P. M., J. Luterbacher, H. von Weissenfluh, E. Xoplaki, M. Brunet, and H. Wanner, 2007: Summer heat waves over western Europe 1880–2003, their relationship to large-scale forcings and predictability. *Climate Dyn.*, **29**, 251–275, doi:10.1007/s00382-007-0233-1.

Diaz, A. F., C. D. Studzinski, and C. R. Mechoso, 1998: Relationships between precipitation anomalies in Uruguay and southern Brazil and sea surface temperature in the Pacific and Atlantic Oceans. *J. Climate*, **11**, 251–271, doi:10.1175/1520-0442(1998)011<0251:RBPAIU>2.0.CO;2.

Ding, Q., B. Wang, J. M. Wallace, and G. Branstator, 2011: Tropical–extratropical teleconnections in boreal summer: Observed interannual variability. *J. Climate*, **24**, 1878–1896, doi:10.1175/2011JCLI3621.1.

Dutra, E., and Coauthors, 2014: Global meteorological drought – Part 2: Seasonal forecasts. *Hydrol. Earth Syst. Sci.*, **18**, 2669–2678, doi:10.5194/hess-18-2669-2014.

Fleig, A. K., L. M. Tallaksen, H. Hisdal, and D. M. Hannah, 2011: Regional hydrological drought in north-western Europe: Linking a new regional drought area index with weather types. *Hydrol. Processes*, **25**, 1163–1179, doi:10.1002/hyp.7644.

Folland, C. K., A. W. Colman, D. P. Rowell, and M. K. Davey, 2001: Predictability of northeast Brazil rainfall and real-time forecast skill, 1987–98. *J. Climate*, **14**, 1937–1958, doi:10.1175/1520-0442(2001)014<1937:PONBRA>2.0.CO;2.

——, J. Knight, H. W. Linderholm, D. Fereday, S. Ineson, and J. W. Hurrell, 2009: The summer North Atlantic Oscillation: Past, present, and future. *J. Climate*, **22**, 1082–1103, doi:10.1175/2008JCLI2459.1.

Funk, C., M. D. Dettinger, J. C. Michaelsen, J. P. Verdin, M. E. Brown, M. Barlow, and A. Hoell, 2008: Warming of the Indian Ocean threatens eastern and southern African food security but could be mitigated by agricultural development. *Proc. Natl. Acad. Sci. USA*, **105**, 11 081–11 086, doi:10.1073/pnas.0708196105.

Gautam, R., N. C. Hsu, W. Lau, and M. Kafatos, 2009: Aerosol and rainfall variability over the Indian monsoon region: Distributions,

trends and coupling. *Ann. Geophys.*, **27**, 3691–3703, doi:10.5194/angeo-27-3691-2009.

Giannini, A., R. Saravanan, and P. Chang, 2004: The preconditioning role of tropical Atlantic variability in the development of the ENSO teleconnection: Implications for the prediction of Nordeste rainfall. *Climate Dyn.*, **22**, 839–855, doi:10.1007/s00382-004-0420-2.

Gillett, N. P., F. W. Zwiers, A. J. Weaver, and P. A. Stott, 2003: Detection of human influence on sea-level pressure. *Nature*, **422**, 292–294, doi:10.1038/nature01487.

Giorgi, F., and P. Lionello, 2008: Climate change projections for the Mediterranean region. *Global Planet. Change*, **63**, 90–104, doi:10.1016/j.gloplacha.2007.09.005.

Goddard, L., A. G. Barnston, and S. J. Mason, 2003: Evaluation of the IRI's "net assessment" seasonal climate forecasts: 1997–2001. *Bull. Amer. Meteor. Soc.*, **84**, 1761–1781, doi:10.1175/BAMS-84-12-1761.

Greve, P., B. Orlowsky, B. Mueller, J. Sheffield, M. Reichstein, and S. I. Seneviratne, 2014: Global assessment of trends in wetting and drying over land. *Nat. Geosci.*, **7**, 716–721, doi:10.1038/ngeo2247.

Hanna, E., T. E. Cropper, P. D. Jones, A. A. Scaife, and R. Allan, 2015: Recent seasonal asymmetric changes in the NAO (a marked summer decline and increased winter variability) and associated changes in the AO and Greenland blocking index. *Int. J. Climatol.*, **35**, 2540–2554, doi:10.1002/joc.4157.

Hartmann, D. L., 2015: Pacific sea surface temperature and the winter of 2014. *Geophys. Res. Lett.*, **42**, 1894–1902, doi:10.1002/2015GL063083.

——, and Coauthors, 2013: Observations: Atmosphere and surface. *Climate Change 2013: The Physical Science Basis*, T. F. Stocker et al., Eds., Cambridge University Press, 159–254.

Hoell, A., and C. Funk, 2013: The ENSO-related west Pacific sea surface temperature gradient. *J. Climate*, **26**, 9545–9562, doi:10.1175/JCLI-D-12-00344.1.

——, and ——, 2014: Indo-Pacific sea surface temperature influences on failed consecutive rainy seasons over eastern Africa. *Climate Dyn.*, **43**, 1645–1660, doi:10.1007/s00382-013-1991-6.

Hoerling, M., and A. Kumar, 2003: The perfect ocean for drought. *Science*, **299**, 691–694, doi:10.1126/science.1079053.

——, J. Eischeid, J. Perlwitz, X. Quan, T. Zhang, and P. Pegion, 2012: On the increased frequency of Mediterranean drought. *J. Climate*, **25**, 2146–2161, doi:10.1175/JCLI-D-11-00296.1.

——, ——, A. Kumar, R. Leung, A. Mariotti, K. Mo, S. Schubert, and R. Seager, 2014: Causes and predictability of the 2012 Great Plains drought. *Bull. Amer. Meteor. Soc.*, **95**, 269–282, doi:10.1175/BAMS-D-13-00055.1.

Huang, R. H., J. L. Chen, and G. Huang, 2007: Characteristics and variations of the East Asian monsoon system and its impacts on climate disasters in China. *Adv. Atmos. Sci.*, **24**, 993–1023, doi:10.1007/s00376-007-0993-x.

Hurrell, J. W., 1995: Decadal trends in the North Atlantic Oscillation: Regional temperatures and precipitation. *Science*, **269**, 676–679, doi:10.1126/science.269.5224.676.

——, J. J. Hack, D. Shea, J. M. Caron, and J. Rosinski, 2008: A new sea surface temperature and sea ice boundary dataset for the Community Atmosphere Model. *J. Climate*, **21**, 5145–5153, doi:10.1175/2008JCLI2292.1.

Iglesias, I., M. N. Lorenzo, and J. J. Taboada, 2014: Seasonal predictability of the east Atlantic pattern from sea surface temperatures. *PLoS One*, **9**, e86439, doi:10.1371/journal.pone.0086439.

Ionita, M., 2014: The impact of the east Atlantic/western Russia pattern on the hydroclimatology of Europe from mid-winter to late spring. *Climate*, **2**, 296–309, doi:10.3390/cli2040296.

IPCC, 2007: *Climate Change 2007: The Physical Science Basis*. Cambridge University Press, 996 pp.

Kaplan, A., M. A. Cane, Y. Kushnir, A. C. Clement, M. B. Blumenthal, and B. Rajagopalan, 1998: Analyses of global sea surface temperature 1856–1991. *J. Geophys. Res.*, **103**, 18 567–18 589, doi:10.1029/97JC01736.

Kelley, C., M. Ting, R. Seager, and Y. Kushnir, 2012: The relative contributions of radiative forcing and internal climate variability to the late 20th century winter drying of the Mediterranean region. *Climate Dyn.*, **38**, 2001–2015, doi:10.1007/s00382-011-1221-z.

Kiehl, J. T., J. J. Hack, G. B. Bonan, B. A. Boville, D. L. Williamson, and P. J. Rasch, 1998: The National Center for Atmospheric Research Community Climate Model: CCM3. *J. Climate*, **11**, 1131–1149, doi:10.1175/1520-0442(1998)011<1131:TNCFAR>2.0.CO;2.

Kim, H. M., P. J. Webster, J. A. Curry, and V. E. Toma, 2012: Asian summer monsoon prediction in ECMWF system 4 and NCEP CFSv2 retrospective seasonal forecasts. *Climate Dyn.*, **39**, 2975–2991, doi:10.1007/s00382-012-1470-5.

Koster, R. D., and Coauthors, 2004: Regions of strong coupling between soil moisture and precipitation. *Science*, **305**, 1138–1140, doi:10.1126/science.1100217.

Kushnir, Y., R. Seager, M. Ting, N. Naik, and J. Nakamura, 2010: Mechanisms of tropical Atlantic SST influence on North American precipitation variability. *J. Climate*, **23**, 5610–5628, doi:10.1175/2010JCLI3172.1.

Lau, K. M., M. K. Kim, and K. M. Kim, 2006: Asian monsoon anomalies induced by aerosol direct effects. *Climate Dyn.*, **26**, 855–864, doi:10.1007/s00382-006-0114-z.

Li, H., A. Dai, T. Zhou, and J. Lu, 2010: Responses of East Asian summer monsoon to historical SST and atmospheric forcing during 1950–2000. *Climate Dyn.*, **34**, 501–514, doi:10.1007/s00382-008-0482-7.

Li, J., R. Yu, W. Yuan, H. Chen, W. Sun, and Y. Zhang, 2015: Precipitation over East Asia simulated by NCAR CAM5 at different horizontal resolutions. *J. Adv. Model. Earth Syst.*, **7**, 774–790, doi:10.1002/2014MS000414.

Li, S. L., J. Lu, G. Huang, and K. M. Hu, 2008: Tropical Indian Ocean basin warming and East Asian summer monsoon: A multiple AGCM study. *J. Climate*, **21**, 6080–6088, doi:10.1175/2008JCLI2433.1.

Liebmann, B., and Coauthors, 2014: Understanding recent eastern Horn of Africa rainfall variability and change. *J. Climate*, **27**, 8630–8645, doi:10.1175/JCLI-D-13-00714.1.

Lloyd-Hughes, B., J. Hannaford, S. Parry, C. Keef, C. Prudhomme, and H. G. Rees, 2010: The spatial coherence of European droughts: UK and Europe drought catalogues. Environment Agency Sci. Rep. SC070079/SR, 64 pp. [Available online at http://nora.nerc.ac.uk/8615/1/SC070079_EA_SR1_EuropeanDroughtCatalogue.pdf.]

Losada, T., B. Rodriguez-Fonseca, E. Mohino, J. Bader, S. Janicot, and C. R. Mechoso, 2012: Tropical SST and Sahel rainfall: A non-stationary relationship. *Geophys. Res. Lett.*, **39**, L12705, doi:10.1029/2012GL052423.

Lyon, B., 2014: Seasonal drought in the greater Horn of Africa and its recent increase during the March–May long rains. *J. Climate*, **27**, 7953–7975, doi:10.1175/JCLI-D-13-00459.1.

——, and D. G. DeWitt, 2012: A recent and abrupt decline in the East African long rains. *Geophys. Res. Lett.*, **39**, L02702, doi:10.1029/2011GL050337.

——, A. G. Barnston, and D. G. DeWitt, 2014: Tropical Pacific forcing of a 1998–99 climate shift: Observational analysis and climate model results for the boreal spring season. *Climate Dyn.*, **43**, 893–909, doi:10.1007/s00382-013-1891-9.

Ma, H.-Y., C. R. Mechoso, Y. Xue, H. Xiao, C.-M. Wu, J.-L. Li, and F. De Sales, 2010: Impact of land surface processes on the South American warm season climate. *Climate Dyn.*, **37**, 187–203, doi:10.1007/s00382-010-0813-3.

Magaña, V., J. A. Amador, and S. Medina, 1999: The mid-summer drought over Mexico and Central America. *J. Climate*, **12**, 1577–1588, doi:10.1175/1520-0442(1999)012<1577:TMDOMA>2.0.CO;2.

Marengo, J. A., and Coauthors, 2008: The drought of Amazonia in 2005. *J. Climate*, **21**, 495–516, doi:10.1175/2007JCLI1600.1.

——, R. Jones, L. M. Alves, and M. C. Valverde, 2009: Future change of temperature and precipitation extremes in South America as derived from the PRECIS regional climate modeling system. *Int. J. Climatol.*, **29**, 2241–2255, doi:10.1002/joc.1863.

Mariotti, A., 2007: How ENSO impacts precipitation in southwest central Asia. *Geophys. Res. Lett.*, **34**, L16706, doi:101029/2007GL030078.

——, and A. Dell'Aquila, 2012: Decadal climate variability in the Mediterranean region: Roles of large-scale forcings and regional processes. *Climate Dyn.*, **38**, 1129–1145, doi:10.1007/s00382-011-1056-7.

——, N. Zeng, J. Yoon, V. Artale, A. Navarra, P. Alpert, and L. Z. X. Li, 2008: Mediterranean water cycle changes: Transition to drier 21st century conditions in observations and CMIP3 simulations. *Environ. Res. Lett.*, **3**, 044001, doi:10.1088/1748-9326/3/4/044001.

——, Y. Pan, N. Zeng, and A. Alessandri, 2015: Long-term climate change in the Mediterranean region in the midst of decadal variability. *Climate Dyn.*, **44**, 1437–1456, doi:10.1007/s00382-015-2487-3.

McCarthy, and Coauthors, 2001: Variability and impacts from El Niño and the Southern Oscillation. *Climate Change 2001: Impacts, Adaptation, and Vulnerability*, J. J. McCarthy et al., Eds., Cambridge University Press, 702–703.

Mechoso, C. R., and S. W. Lyons, 1988: On the atmospheric response to SST anomalies associated with the Atlantic warm event during 1984. *J. Climate*, **1**, 422–428, doi:10.1175/1520-0442(1988)001<0422:OTARTS>2.0.CO;2.

——, and Coauthors, 1995: The seasonal cycle over the tropical Pacific in coupled ocean–atmosphere general circulation models. *Mon. Wea. Rev.*, **123**, 2825–2838, doi:10.1175/1520-0493(1995)123<2825:TSCOTT>2.0.CO;2.

Mo, K. C., and E. H. Berbery, 2011: Drought and persistent wet spells over South America based on observations and the U.S. CLIVAR drought experiments. *J. Climate*, **24**, 1801–1820, doi:10.1175/2010JCLI3874.1.

Mohino, E., S. Janicot, and J. Bader, 2011a: Sahelian rainfall and decadal to multidecadal SST variability. *Climate Dyn.*, **37**, 419–440, doi:10.1007/s00382-010-0867-2.

——, B. Rodríguez-Fonseca, T. Losada, S. Gervois, S. Janicot, J. Bader, P. Ruti, and F. Chauvin, 2011b: Changes in the interannual SST-forced signals on West African rainfall. AGCM intercomparison. *Climate Dyn.*, **37**, 1707–1725, doi:10.1007/s00382-011-1093-2.

Molod, A., L. Takacs, M. Suarez, J. Bacmeister, I.-S. Song, and A. Eichmann, 2012: The GEOS-5 atmospheric general circulation model: Mean climate and development from MERRA to Fortuna. NASA Tech. Rep. Series on Global Modeling and Data Assimilation, Vol. 28, NASA TM-2012-104606, 117 pp.

Mueller, B., and S. I. Seneviratne, 2012: Hot days induced by precipitation deficits at the global scale. *Proc. Natl. Acad. Sci. USA*, **109**, 12 398–12 403, doi:10.1073/pnas.1204330109.

Müller, O. V., E. H. Berbery, D. Alcaraz-Segura, and M. B. Ek, 2014: Regional model simulations of the 2008 drought in southern South America using a consistent set of land surface properties. *J. Climate*, **27**, 6754–6778, doi:10.1175/JCLI-D-13-00463.1.

Orlowsky, B., and S. I. Seneviratne, 2012: Global changes in extreme events: Regional and seasonal dimension. *Climatic Change*, **110**, 669–696, doi:10.1007/s10584-011-0122-9.

——, and ——, 2013: Elusive drought: Uncertainty in observed trends and short- and long-term CMIP5 projections. *Hydrol. Earth Syst. Sci.*, **17**, 1765–1781, doi:10.5194/hess-17-1765-2013.

Orth, R., and S. I. Seneviratne, 2013: Predictability of soil moisture and streamflow on sub-seasonal timescales: A case study. *J. Geophys. Res. Atmos.*, **118**, 10 963–10 979, doi:10.1002/jgrd.50846.

Parry, S., J. Hannaford, B. Lloyd-Hughes, C. Prudhomme, and C. Keef, 2010: Drought summaries of spatio-temporal evolution of major European droughts since 1960. Environment Agency Sci. Rep. SC070079.

Poveda, G., and O. J. Mesa, 1997: Feedbacks between hydrological processes in tropical South America and large-scale ocean–atmospheric phenomena. *J. Climate*, **10**, 2690–2702, doi:10.1175/1520-0442(1997)010<2690:FBHPIT>2.0.CO;2.

Qian, C., and T. Zhou, 2014: Multidecadal variability of north China aridity and its relationship to PDO during 1900–2010. *J. Climate*, **27**, 1210–1222, doi:10.1175/JCLI-D-13-00235.1.

Ramanathan, V., and Coauthors, 2005: Atmospheric brown clouds: Impacts on south Asian climate and hydrological cycle. *Proc. Natl. Acad. Sci. USA*, **102**, 5326–5333, doi:10.1073/pnas.0500656102.

Rayner, N. A., D. E. Parker, E. B. Horton, C. K. Folland, L. V. Alexander, D. P. Rowell, E. C. Kent, and A. Kaplan, 2003: Global analyses of sea surface temperature, sea ice, and night marine air temperature since the late nineteenth century. *J. Geophys. Res.*, **108**, 4407, doi:10.1029/2002JD002670.

Richter, I., 2015: Climate model biases in the eastern tropical oceans: Causes, impacts and ways forward. *Wiley Interdiscip. Rev.: Climate Change*, **6**, 345–358, doi:10.1002/wcc.338.

Rienecker, M. M., and Coauthors, 2008: The GEOS-5 data assimilation system—Documentation of versions 5.0.1, 5.1.0, and 5.2.0. NASA Tech. Rep. Series on Global Modeling and Data Assimilation, Vol. 27, NASA/TM-2007-104606, 98 pp. [Available online at http://gmao.gsfc.nasa.gov/pubs/docs/Rienecker369.pdf.]

Robson, J., R. Sutton, K. Lohmann, D. Smith, and M. Palmer, 2012: The causes of the rapid warming of the North Atlantic Ocean in the mid-1990s. *J. Climate*, **25**, 4116–4134, doi:10.1175/JCLI-D-11-00443.1.

Rodell, M., and Coauthors, 2004: The Global Land Data Assimilation System. *Bull. Amer. Meteor. Soc.*, **85**, 381–394, doi:10.1175/BAMS-85-3-381.

Rodríguez-Fonseca, B., I. Polo, J. García-Serrano, T. Losada, E. Mohino, C. R. Mechoso, and F. Kucharski, 2009: Are Atlantic Niños enhancing Pacific ENSO events in recent decades? *Geophys. Res. Lett.*, **36**, L20705, doi:10.1029/2009GL040048.

——, and Coauthors, 2011: Interannual and decadal SST-forced responses of the West African monsoon. *Atmos. Sci. Lett.*, **12**, 67–74, doi:10.1002/asl.308.

——, and Coauthors, 2015: Variability and predictability of West African droughts: A review of the role of sea surface temperature anomalies. *J. Climate*, **28**, 4034–4060, doi:10.1175/JCLI-D-14-00130.1.

Roeckner, E., and Coauthors, 2003: The atmospheric general circulation model ECHAM5. Part I: Model description. Max

Planck Institute for Meteorology Rep. 349, 127 pp. [Available from MPI for Meteorology, Bundesstr. 53, 20146 Hamburg, Germany.]

Ropelewski, C. F., and M. S. Halpert, 1987: Global and regional scale precipitation patterns associated with the El Niño/Southern Oscillation. *Mon. Wea. Rev.*, **115**, 1606–1626, doi:10.1175/1520-0493(1987)115<1606:GARSPP>2.0.CO;2.

Rowell, D. P., 2013: Simulating SST teleconnections to Africa: What is the state of the art? *J. Climate*, **26**, 5397–5418, doi:10.1175/JCLI-D-12-00761.1.

Sánchez, E., and Coauthors, 2015: Regional climate modelling in CLARIS-LPB: A concerted approach towards twenty-first century projections of regional temperature and precipitation over South America. *Climate Dyn.*, **45**, 2193–2212, doi:10.1007/s00382-014-2466-0.

Saravanan, R., and P. Chang, 2000: Interaction between tropical Atlantic variability and El Niño–Southern Oscillation. *J. Climate*, **13**, 2177–2194, doi:10.1175/1520-0442(2000)013<2177:IBTAVA>2.0.CO;2.

Scaife, A. A., J. R. Knight, G. K. Vallis, and C. K. Folland, 2005: A stratospheric influence on the winter NAO and North Atlantic surface climate. *Geophys. Res. Lett.*, **32**, L18715, doi:10.1029/2005GL023226.

Schubert, S. D., M. J. Suarez, P. J. Pegion, R. D. Koster, and J. T. Bacmeister, 2004: On the cause of the 1930s Dust Bowl. *Science*, **303**, 1855–1859, doi:10.1126/science.1095048.

——, and Coauthors, 2009: A U.S. CLIVAR project to assess and compare the responses of global climate models to drought-related SST forcing patterns: Overview and results. *J. Climate*, **22**, 5251–5272, doi:10.1175/2009JCLI3060.1.

——, H. Wang, and M. Suarez, 2011: Warm season subseasonal variability and climate extremes in the Northern Hemisphere: The role of stationary Rossby waves. *J. Climate*, **24**, 4773–4792, doi:10.1175/JCLI-D-10-05035.1.

——, ——, R. Koster, M. Suarez, and P. Groisman, 2014: Northern Eurasian heat waves and droughts. *J. Climate*, **27**, 3169–3207, doi:10.1175/JCLI-D-13-00360.1.

Seager, R., and M. Hoerling, 2014: Atmosphere and ocean origins of North American drought. *J. Climate*, **27**, 4581–4606, doi:10.1175/JCLI-D-13-00329.1.

——, Y. Kushnir, C. Herweijer, N. Naik, and J. Velez, 2005: Modeling the tropical forcing of persistent droughts and pluvials over western North America: 1856–2000. *J. Climate*, **18**, 4068–4091, doi:10.1175/JCLI3522.1.

——, N. Naik, W. Baethgen, A. Robertson, Y. Kushnir, J. Nakamura, and S. Jurburg, 2010: Tropical oceanic causes of interannual to multidecadal precipitation variability in southeast South America over the past century. *J. Climate*, **23**, 5517–5539, doi:10.1175/2010JCLI3578.1.

——, L. Goddard, J. Nakamura, N. Henderson, and D. E. Lee, 2014a: Dynamical causes of the 2010/11 Texas–northern Mexico drought. *J. Hydrometeor.*, **15**, 39–68, doi:10.1175/JHM-D-13-024.1.

——, H. Liu, N. Henderson, I. Simpson, C. Kelley, T. Shaw, Y. Kushnir, and M. Ting, 2014b: Causes of increasing aridification of the Mediterranean region in response to rising greenhouse gases. *J. Climate*, **27**, 4655–4676, doi:10.1175/JCLI-D-13-00446.1.

——, M. Hoerling, S. Schubert, H. Wang, B. Lyon, A. Kumar, J. Nakamura, and N. Henderson, 2014c: Causes and predictability of the 2011–14 California drought. DTF/NIDIS Assessment Rep., 40 pp. [Available online at http://cpo.noaa.gov/MAPP/californiadroughtreport.]

Seneviratne, S. I., and Coauthors, 2006: Soil moisture memory in AGCM simulations: Analysis of Global Land–Atmosphere Coupling Experiment (GLACE) data. *J. Hydrometeor.*, **7**, 1090–1112, doi:10.1175/JHM533.1.

——, and Coauthors, 2012a: Changes in climate extremes and their impacts on the natural physical environment. *Managing the Risks of Extreme Events and Disasters to Advance Climate Change Adaptation*, C. B. Field et al., Eds., IPCC, 109–230.

——, and Coauthors, 2012b: Swiss prealpine Rietholzbach research catchment and lysimeter: 32-year time series and 2003 drought. *Water Resour. Res.*, **48**, W06526, doi:10.1029/2011WR011749.

Sheffield, J., E. F. Wood, and M. L. Roderick, 2012: Little change in global drought in the past 60 years. *Nature*, **491**, 435–438, doi:10.1038/nature11575.

Smith, D. M., A. A. Scaife, and B. P. Kirtman, 2012: What is the current state of knowledge with regard to seasonal to decadal forecasting? *Environ. Res. Lett.*, **7**, 015602, doi:10.1088/1748-9326/7/1/015602.

Song, F., and T. Zhou, 2014a: Interannual variability of East Asian summer monsoon simulated by CMIP3 and CMIP5 AGCMs: Skill dependence on Indian Ocean–western Pacific anticyclone teleconnection. *J. Climate*, **27**, 1679–1697, doi:10.1175/JCLI-D-13-00248.1.

——, and ——, 2014b: The climatology and interannual variability of East Asian summer monsoon in CMIP5 coupled models: Does air–sea coupling improve the simulations? *J. Climate*, **27**, 8761–8777, doi:10.1175/JCLI-D-14-00396.1.

——, ——, and Y. Qian, 2014: Responses of East Asian summer monsoon to natural and anthropogenic forcings in the 17 latest CMIP5 models. *Geophys. Res. Lett.*, **41**, 596–603, doi:10.1002/2013GL058705.

Sörensson, A. A., and C. G. Menéndez, 2011: Summer soil–precipitation coupling in South America. *Tellus*, **63A**, 56–68, doi:10.1111/j.1600-0870.2010.00468.x.

Spinoni, J., G. Naumann, J. Vogt, and P. Barbosa, 2015: The biggest drought events in Europe from 1950 to 2012. *J. Hydrol.*, **3**, 509–524, doi:10.1016/j.ejrh.2015.01.001.

Stagge, J. H., I. Kohn, L. M. Tallaksen, and K. Stahl, 2015: Modeling drought impact occurrence based on meteorological drought indices in Europe. *J. Hydrol.*, **530**, 37–50, doi:10.1016/j.jhydrol.2015.09.039.

Stahl, K., 2001: Hydrological drought—A study across Europe. Ph.D. thesis, Albert-Ludwigs-Universität Freiburg, Freiburger Schriften zur Hydrologie 15, 122 pp.

Staudinger, M., K. Stahl, and J. Seibert, 2014: A drought index accounting for snow. *Water Resour. Res.*, **50**, 7861–7872, doi:10.1002/2013WR015143.

Sutton, R., and B. Dong, 2012: Atlantic Ocean influence on a shift in European climate in the 1990s. *Nat. Geosci.*, **5**, 788–792, doi:10.1038/ngeo1595.

Tallaksen, L. M., J. H. Stagge, K. Stahl, L. Gudmundsson, R. Orth, S. I. Seneviratne, A. F. Van Loon, and H. A. J. Van Lanen, 2015: Characteristics and drivers of drought in Europe—A summary of the DROUGHT-RSPI project. *Drought: Research and Science-Policy Interfacing*, Andreu et al., Eds., Taylor and Francis Group, 15–22.

Teuling, A. J., and Coauthors, 2013: Evapotranspiration amplifies European summer drought. *Geophys. Res. Lett.*, **40**, 2071–2075, doi:10.1002/grl.50495.

Van Loon, A. F., and H. A. Van Lanen, 2012: A process-based typology of hydrological drought. *Hydrol. Earth Syst. Sci.*, **16**, 1915–1946, doi:10.5194/hess-16-1915-2012.

Vicente-Serrano, S. M., S. Beguería, and J. I. López-Moreno, 2010: A multiscalar drought index sensitive to global warming: The standardized precipitation evapotranspiration index. *J. Climate*, **23**, 1696–1718, doi:10.1175/2009JCLI2909.1.

Wang, C., S.-K. Lee, and D. B. Enfield, 2008: Climate response to anomalously large and small Atlantic warm pools during the summer. *J. Climate*, **21**, 2437–2450, doi:10.1175/2007JCLI2029.1.

Wang, G., Y. Kim, and D. Wang, 2007: Quantifying the strength of soil moisture–precipitation coupling and its sensitivity to changes in surface water budget. *J. Hydrometeor.*, **8**, 551–570, doi:10.1175/JHM573.1.

Wang, H., S. D. Schubert, M. J. Suarez, J. Chen, M. Hoerling, A. Kumar, and P. Pegion, 2009: Attribution of the seasonality and regionality in climate trends over the United States during 1950–2000. *J. Climate*, **22**, 2571–2590, doi:10.1175/2008JCLI2359.1.

——, ——, R. Koster, Y.-G. Ham, and M. Suarez, 2014: On the role of SST forcing in the 2011 and 2012 extreme U.S. heat and drought: A study in contrasts. *J. Hydrometeor.*, **15**, 1255–1273, doi:10.1175/JHM-D-13-069.1.

Wu, B., T. Zhou, and T. Li, 2009: Seasonally evolving dominant interannual variability modes of East Asian climate. *J. Climate*, **22**, 2992–3005, doi:10.1175/2008JCLI2710.1.

——, T. Li, and T. Zhou, 2010: Relative contributions of the Indian Ocean and local SST anomalies to the maintenance of the western North Pacific anomalous anticyclone during El Niño decaying summer. *J. Climate*, **23**, 2974–2986, doi:10.1175/2010JCLI3300.1.

Wu, R., Z. Hu, and B. Kirtman, 2003: Evolution of ENSO-related rainfall anomalies in East Asia. *J. Climate*, **16**, 3742–3758, doi:10.1175/1520-0442(2003)016<3742:EOERAI>2.0.CO;2.

Xie, S.-P., K. Hu, J. Hafner, H. Tokinaga, Y. Du, G. Huang, and T. Sampe, 2009: Indian Ocean capacitor effect on Indo–western Pacific climate during the summer following El Niño. *J. Climate*, **22**, 730–747, doi:10.1175/2008JCLI2544.1.

Xoplaki, E., J. F. Gonzalez-Rouco, and J. Luterbacher, 2004: Wet season Mediterranean precipitation variability: Influence of large-scale dynamics and trends. *Climate Dyn.*, **23**, 63–78, doi:10.1007/s00382-004-0422-0.

Xue, Y., F. de Sales, C. R. Mechoso, C. A. Nobre, and H.-M. Juang, 2006: Role of land surface processes in South American monsoon development. *J. Climate*, **19**, 741–762, doi:10.1175/JCLI3667.1.

Yang, F. L., and K. M. Lau, 2004: Trend and variability of China precipitation in spring and summer: Linkage to sea-surface temperatures. *Int. J. Climatol.*, **24**, 1625–1644, doi:10.1002/joc.1094.

Yang, W., R. Seager, M. A. Cane, and B. Lyon, 2014: The East African long rains in observations and models. *J. Climate*, **27**, 7185–7202, doi:10.1175/JCLI-D-13-00447.1.

Yin, D., M. L. Roderick, G. Leech, F. Sun, and Y. Huang, 2014: The contribution of reduction in evaporative cooling to higher surface air temperatures during drought. *Geophys. Res. Lett.*, **41**, 7891–7897, doi:10.1002/2014GL062039.

Yoon, J.-H., and N. Zeng, 2010: An Atlantic influence on Amazon rainfall. *Climate Dyn.*, **34**, 249–264, doi:10.1007/s00382-009-0551-6.

Zeng, N., J. D. Neelin, K.-M. Lau, and C. J. Tucker, 1999: Enhancement of interdecadal climate variability in the Sahel by vegetation interaction. *Science*, **286**, 1537–1540, doi:10.1126/science.286.5444.1537.

Zhang, L., and T. Zhou, 2015: Drought over East Asia: A review. *J. Climate*, **28**, 3375–3399, doi:10.1175/JCLI-D-14-00259.1.

Zhou, T., R. Yu, H. Li, and B. Wang, 2008a: Ocean forcing to changes in global monsoon precipitation over the recent half-century. *J. Climate*, **21**, 3833–3852, doi:10.1175/2008JCLI2067.1.

——, L. Zhang, and H. Li, 2008b: Changes in global land monsoon area and total rainfall accumulation over the last half century. *Geophys. Res. Lett.*, **35**, L16707, doi:10.1029/2008GL034881.

——, D. Gong, J. Li, and B. Li, 2009a: Detecting and understanding the multi-decadal variability of the East Asian summer monsoon—Recent progress and state of affairs. *Meteor. Z.*, **18**, 455–467, doi:10.1127/0941-2948/2009/0396.

——, B. Wu, and B. Wang, 2009b: How well do atmospheric general circulation models capture the leading modes of the interannual variability of the Asian–Australian monsoon? *J. Climate*, **22**, 1159–1173, doi:10.1175/2008JCLI2245.1.

Zhou, and Coauthors, 2009c: The CLIVAR C20C project: Which components of the Asian–Australian monsoon circulation variations are forced and reproducible? *Climate Dyn.*, **33**, 1051–1068, doi:10.1007/s00382-008-0501-8.

Zhou, T., F. Song, R. Lin, X. Chen, and X. Chen, 2013: The 2012 north China floods: Explaining an extreme rainfall event in the context of a long-term drying tendency. *Bull. Amer. Meteor. Soc.*, **94** (9), S49–S51, doi:10.1175/BAMS-D-13-00085.1.

Zwiers, F. W., X. L. Wang, and J. Sheng, 2000: Effects of specifying bottom boundary conditions in an ensemble of atmospheric GCM simulations. *J. Geophys. Res.*, **105**, 7295–7315, doi:10.1029/1999JD901050.